Final Report

Project Title

CRC 2020 P0039

Behavior and Design of Concrete Structures under Natural Fire

Prepared for the ACI Foundation

Authors

Thomas Gernay, Ph.D.
Assistant Professor
Johns Hopkins University

Patrick Bamonte, Ph.D.
Associate Professor
Politecnico di Milano

Project start date: 1 November 2020
Final Report Delivery Date: 31 January 2022

(a) Acknowledgement of Support

This report is based upon work supported by the ACI Foundation, research grant # CRC 2020 P0039. This support is gratefully acknowledged.

The project is supported by an advisory team composed of the following members:

- Ann Masek, ACI Foundation
- Tricia Ladely, ACI Foundation
- Fabienne Robert, CERIB, Convenor CEN TC 250/SC2/WG1/TG5
- Kevin Mueller, Thornton Tomasetti, Chair of ACI 216

The members of the advisory team and members of ACI 216 are sincerely thanked for their generous input.

(b) Disclaimer

All research, summaries, opinions, findings, conclusions and recommendations expressed in this report are those of the authors and do not necessarily reflect those of the American Concrete Institute, the ACI Foundation, the members of the advisory team, or other sponsors, institutions, agencies or organizations which may have supported this research. Mention of trade names or commercial products does not constitute their endorsement by ACI or other sponsors.

Under a license agreement between Gesval S.A. and the Johns Hopkins University, Dr. Gernay and the Johns Hopkins University are entitled to royalty distributions related to the technology SAFIR described in the study discussed in this report. This arrangement has been reviewed and approved by the Johns Hopkins University in accordance with its conflict of interest policies.

Table of Contents

1. Introduction

The current fire resistance design strategy for building structures is based on the consideration of a standard time-temperature exposure (such as ASTM 119 [1]) which is monotonically increasing, i.e., consists in heating up the member until it fails. While this implicitly aims at ensuring that buildings remain stable for enough time to allow evacuation, it does not contemplate the issue of structural integrity during and after the decay phases of the fire. This is a shortcoming because, as a result, the current fire designs fail to address the possibility of structural collapse after the time of peak gas temperature under real fires.

Recently, performance objectives for the built environment under extreme hazards are extending from life safety of building occupants to broader resilience requirements. It is now a societal expectation that, in case of disaster, first responders can intervene safely and the building can remain standing, and even possibly re-occupied after the event. Yet, meeting these expectations for fire hazard requires complementing/extending the current fire resistance rating system with a new paradigm, since the current design methods are based on an oversimplification of the time-temperature exposure.

The objective of this research is to develop a design method for concrete structural members subjected to fire that allows achieving resistance to full burnout under real fires. The novel method aims at capturing the effects of heating and cooling through the entire fire duration on the members. The objective is not to replace advanced analysis for performance-based assessment, but to provide a new simple method, of straightforward application for design by practitioners, which addresses the need for burnout resistant structural design. The method is intended to complement the fire resistance rating. The two indicators of *fire resistance* rating and *burnout resistance* rating would then provide a holistic picture of the structural response under the different stages of a fire including the vulnerability to delayed structural failure. As a result, performance requirements may encompass not only the event alone, but also the phases after the event.

To achieve the objective, the research work is divided in four tasks:

1) Experimental testing of material specimens to characterize thermal and mechanical properties during the cooling phase and in residual conditions;
2) Selection of 'standardized' design fire scenarios that include the cooling phases;
3) Numerical parametric analyses by the finite element method to quantify the thermo-mechanical response of prototypical concrete members under the design fire scenarios; and
4) Derivation of tabulated data and simple design methods for evaluating the *burnout resistance* rating of concrete members.

This project is carried out by Dr. Thomas Gernay at Johns Hopkins University and Dr. Patrick Bamonte at Politecnico di Milano, with support from ACI Foundation research grant # CRC 2020 P0039. This report summarizes the research works and findings from the project, which was conducted between November 2020 and January 2022.

2. Experimental Tests on Concrete Specimens subject to Heating and Cooling

2.1 Concrete specimens

Prior to the beginning of the project, it was decided to focus on two types of concrete, characterized by the two most common types of aggregate: siliceous and calcareous.

The siliceous concrete was cast at Politecnico di Milano (Milan, Italy) at the beginning of September 2020. The concrete containing mostly calcareous aggregate was cast at CERIB (Epernon, France) towards the end of October 2020. Following the compressive tests carried out at 28 days on the concrete cast at CERIB, it was decided to cast two more concretes (both containing mostly calcareous aggregate), in January 2021 at CERIB.

The specimens are shown in Figure 1 and Figure 2. For each concrete batch, the following specimens were cast:

- 30 cylinders (diameter = 100 mm, height = 300 mm) for the mechanical tests;
- 4 or 5 cylinders (diameter = 100 mm, height = 300 mm) for measuring the thermal diffusivity. These specimens were equipped with two thermocouples that were placed inside the molds prior to casting.

Additional specimens were cast for quality control (early-stage tests to monitor the in-time evolution of the compressive strength) and for thermal dilation tests (to be carried out in future research programs).

Mix proportions are listed in Table 1. For the three concretes cast at CERIB, the sand was mostly calcareous (> 50%), in accordance with the definitions of calcareous concrete given in the standards. The compressive strength values reported in the table refers to the tests at 28 days, and was measured on small cubes ($100 \times 100 \times 100$ mm^3) in the case of the siliceous concrete, while for the mostly calcareous concretes large cylinders (diameter = 160 mm, height = 320 mm) were used. For the sake of comparison, the values of cube strength were converted to cylinder strength by means of a widely accepted empirical formulae (where the cylindrical strength is 83% of the corresponding cubic strength). During the experimental campaign, further tests on cylinders were carried out to test the in-time evolution of the compressive strength, and the values reported in Table 1 were confirmed.

Figure 1. Concrete specimens of the first concrete batch (siliceous concrete).

Figure 2. Concrete specimens of the third and fourth concrete batch (mostly calcareous concretes).

Table 1. Mix proportions (* mostly calcareous).

	Mix 1 (S)	**Mix 2 (C1)**	**Mix 3 (C2)**	**Mix 4 (C3)**
casting date	09/08/2020	10/23/2020	11/01/2021	26/01/2021
aggregate	siliceous	calcareous	calcareous	calcareous
sand (0-4 mm) [kg]	965	973	1071	1060
gravel (4-10 mm) [kg]	695	819	771	771
cement (CEM I) [kg]	350	350	350	350
water [l]	185	149	100	120
superplasticizer [%]	1.0	1.15	1.15	1.15
PP fibers	-	yes	-	yes
density [kg/m^3]	2346	2024	2137	1999
compressive strength [MPa]	34.4	29.5	47.5	31.3

The specimens used for quality control and for measuring the reference compressive strength at 28 days were all stored in vapor-saturated environment (relative humidity RH > 98%). All the other specimens were stored in conditions complying with the provisions of the RILEM draft recommendation “129-MHT Test methods for mechanical properties of concrete at high temperatures”, namely:

- in a room with vapor-saturated environment for the first 7 days;
- in controlled environment at 20°C and RH = 50% up to the day of testing.

The specimens for the mechanical tests were cut and ground (in order to guarantee the planarity of the end faces) two months before the tests. A further check of the quality and homogeneity of the concrete batches was carried out by measuring the density of the specimens after their preparation. The results are shown in Figure 3 in the form of density distributions. It is worth noting that, in all cases, a rather low coefficient of variation (COV) was found, with the value obtained for the siliceous concrete (Figure 3a) strongly affected by one single specimen with density lower than the others (due to poor casting). Moreover, in the case of the second mix (Figure 3b) a very low value of density was found; this fact was attributed to the presence of polypropylene fibers in the mix and motivated the decision of casting two more concretes (one of which without fibers). It turned out, however, that also the fourth concrete batch (C3), also containing polypropylene fibers, exhibited a rather low density (average value = 1999 kg/m^3). Despite this low value of density, and given the closeness between its compressive strength and that of the siliceous concrete, C3 was chosen as reference concrete batch for the high temperature tests.

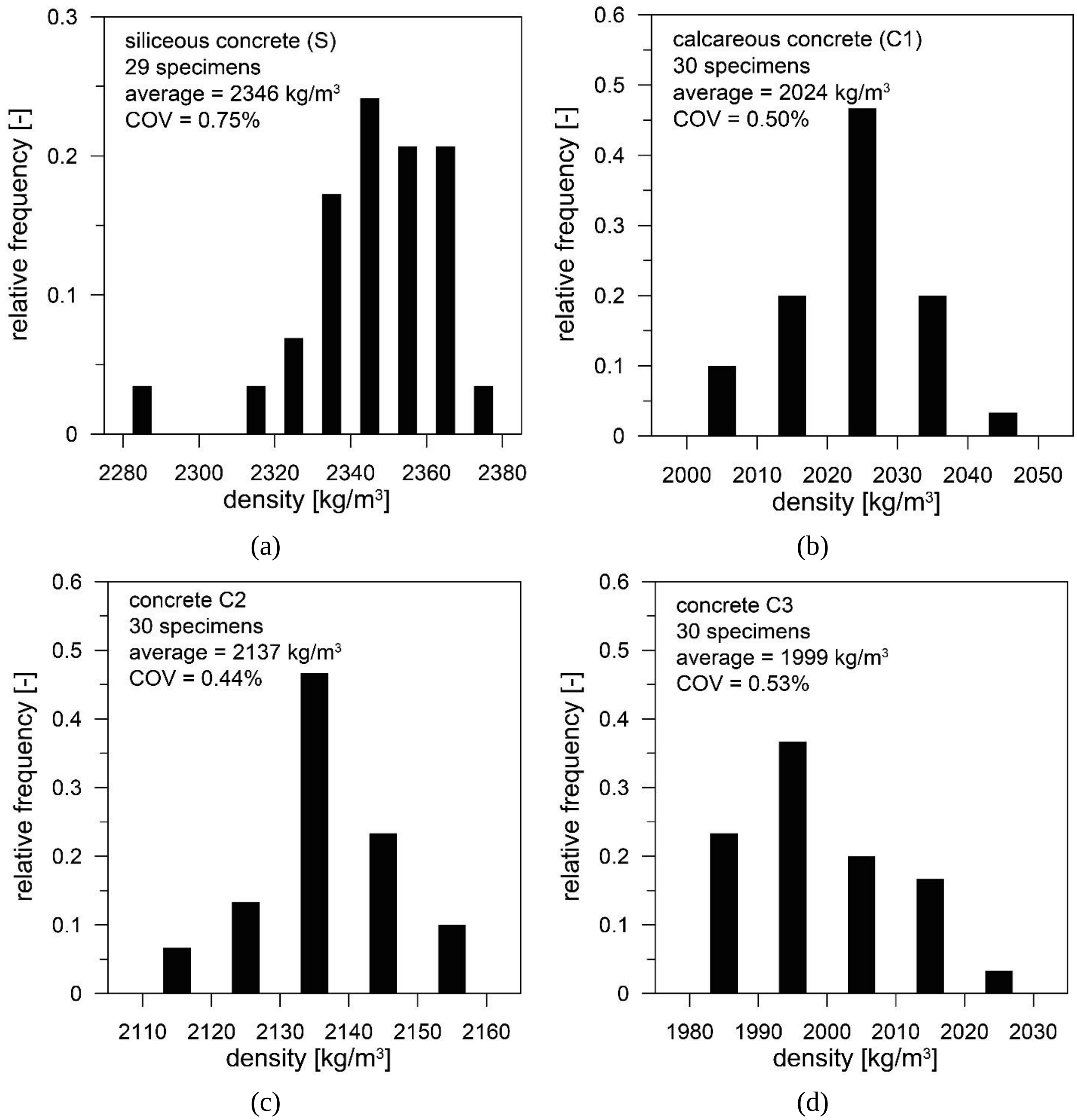

Figure 3. Density distribution of the four concrete batches: (a) siliceous concrete (S); (b) calcareous concrete C1; (c) calcareous concrete C2; (d) calcareous concrete C3.

2.2 Thermal properties tests

The thermal characterization was carried out by measuring the thermal diffusivity. Thermal diffusivity is the main property in transient problems involving conduction as the main heat-transfer mechanism, such as reinforced concrete sections.

For both concrete batches, five elongated cylinders (∅ = 100 mm, h = 300 mm) were used. Before casting, two thermocouples were placed inside each cylinder by means of nylon wires, with their axis parallel to the longitudinal axis of the cylinder. One thermocouple was placed very close to the lateral surface and the other along the axis, both reaching the mid-height section of the specimens.

The specimens were then heated inside an electric furnace, at slow heating rates (1-2°C/min) up to a maximum temperature of 750 or 900°C depending on the specimen. The parameters were varied to ascertain the sensitivity of the measurements to the different parameters. The position inside the furnace as well as the length of the specimens guarantee an axisymmetric temperature distribution inside the specimens and allow to evaluate the diffusivity on the basis of the temperatures measured by the two thermocouples, assuming a one-dimensional heat transfer governed by the radial coordinate (measured from the center of the specimen). The length of the specimen, together with the placement of the thermocouple measuring tip at mid-length, rules out the role played by heat transfer at the end faces of the specimen.

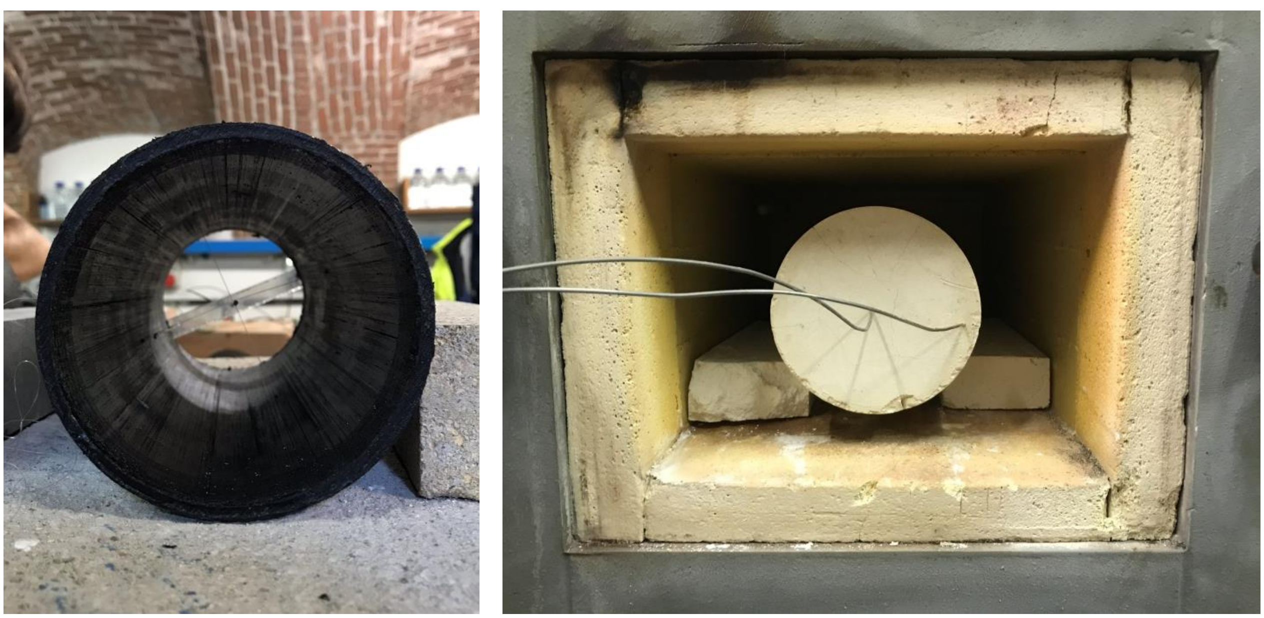

(a) (b)

Figure 4. (a) Preparation of the moulds; (b) specimen inside the electric furnace prior to testing.

A complete overview of the completed thermal diffusivity tests is shown in Table 2. In addition to the thermal diffusivity, the specimens also allowed the measurement of the density prior and after the tests and thus to monitor the mass loss.

Table 2. Summary of the thermal diffusivity tests.

specimen	test date	heating rate [°C/min]	mass loss [%]
S-D1	01/13/2021	1.00	-9
S-D2	01/22/2021	2.00	-13
S-D4	02/09/2021	1.00	-14
C1-D1	02/18/2021	2.00	-22
C1-D2	02/24/2021	2.00	-11

As previously mentioned, the thermal parameter controlling heat transfer by conduction is the thermal diffusivity D, which represents the ratio between the heat transmitted and the heat stored by the unit mass of the material under a unit thermal gradient and in a unit time: $D = \lambda/(c\ \rho)$, where λ is the thermal conductivity, c is the specific heat and ρ is the mass per unit volume; D [m^2/s]. In long cylinders ($h \geq 2\varnothing$), such as the ones used in the present project, subjected to a constant heating rate (v_h = mean heating rate inside the specimen), the thermal diffusivity can be evaluated by means of the following equation:

$$D = v_h\ R^2/(4\ \Delta T)$$

where $\Delta T = T_2 - T_1$ is the difference between the temperatures measured by the two thermocouples and R is the distance between their axes (Figure 4b). Since the heating rate is not constant inside the specimens, v_h in the previous equation is obtained by calculating a weighted average between the heating rates measured at the two thermocouples.

The typical results obtained during the tests are shown in Figure 5 for specimen S-D2. For the sake of comparison, in accordance with the main objectives of the experimental program, the heating phase (left) is plotted separately from the cooling phase (right). The change of state of the free water from liquid to vapor in the micropores, and the change in the crystalline system (from α to β) of the quartz contained in the fine aggregates are responsible for the downward spikes at 100-200°C and 550-580°C, respectively. These effects are commonly observed in diffusivity tests. On the contrary, the plot of the cooling phase highlights the irreversible behavior of the material.

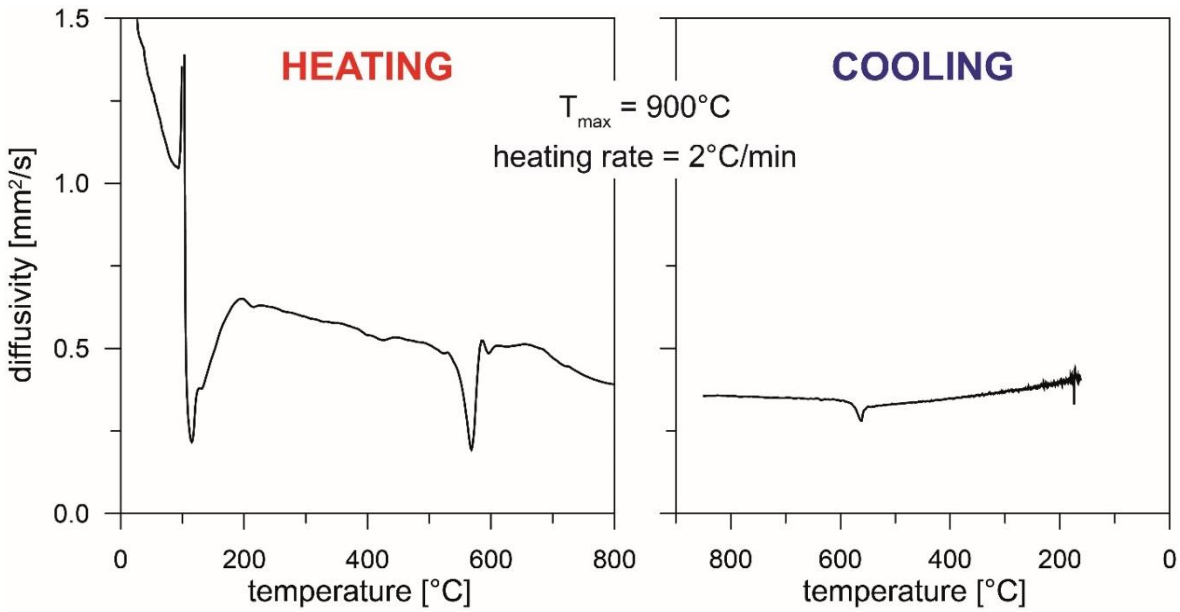

Figure 5. Thermal diffusivity of specimen S-D2 in the heating (left) and cooling phase (right).

The results of all the tests are plotted in Figure 6, together with the provisions contained in EN1992-1-2 [2]. The considerations drawn for specimen S-D2 also hold for the other specimens. Noteworthy, the behavior in the cooling phase is mostly irreversible, regardless of heating/cooling rate and maximum temperature reached during the tests.

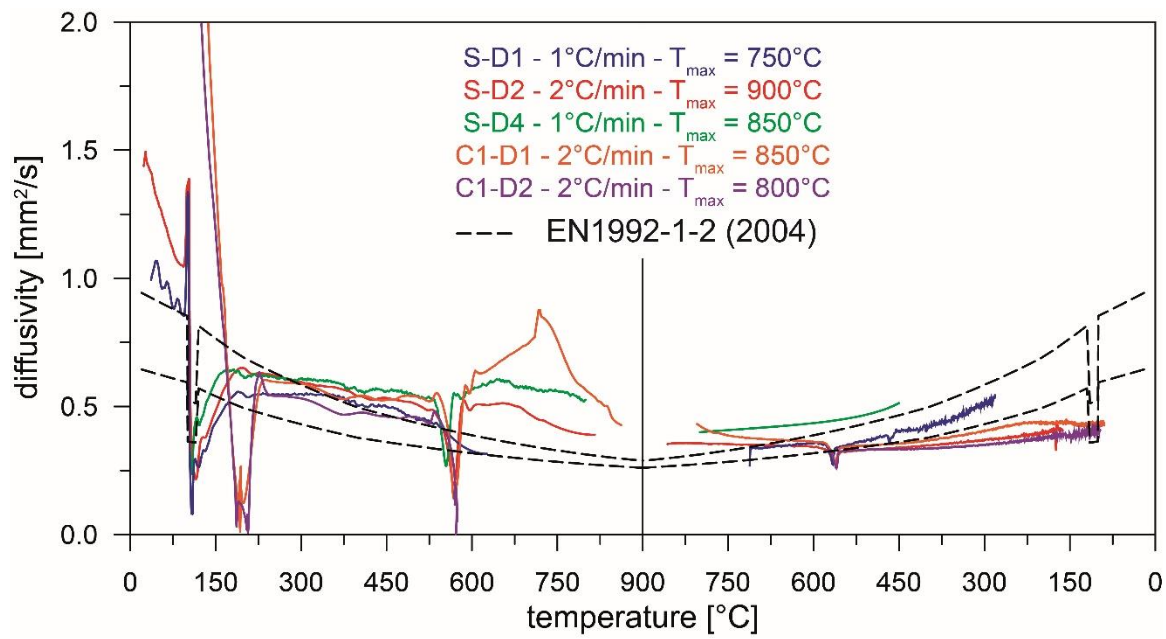

Figure 6. Results from the thermal diffusivity tests in heating and cooling.

To complement the experiments, the thermal diffusivity tests were then simulated numerically. This was done with the two-fold objective of (a) checking whether the values of diffusivity measured are adequate to represent the conduction phenomenon inside the specimens tested; (b) compare the diffusivity measured with the provisions of Eurocode (prEN1992-1-2, which contains the most updated version, calibrated on the basis of numerous test results).

The simulations were carried out by means of the FE commercial software ABAQUS. Considering that the aim is to focus on conduction, only the portion of the specimens between the two thermocouples was modelled. This is instrumental for ruling out the effects of the boundary conditions on the exposed surface (i.e., mostly radiation in the electric furnace). To this end, a fictitious cylindrical boundary was defined, with a radius of 45 mm, i.e., the position of the external thermocouple (T_{ext} in Figure 7a-b). The fictitious boundary is highlighted in Figure 7b by means of a dashed line. Along the fictitious boundary, the temperature measured by the external thermocouple was imposed as boundary condition (Dirichlet-type boundary condition).

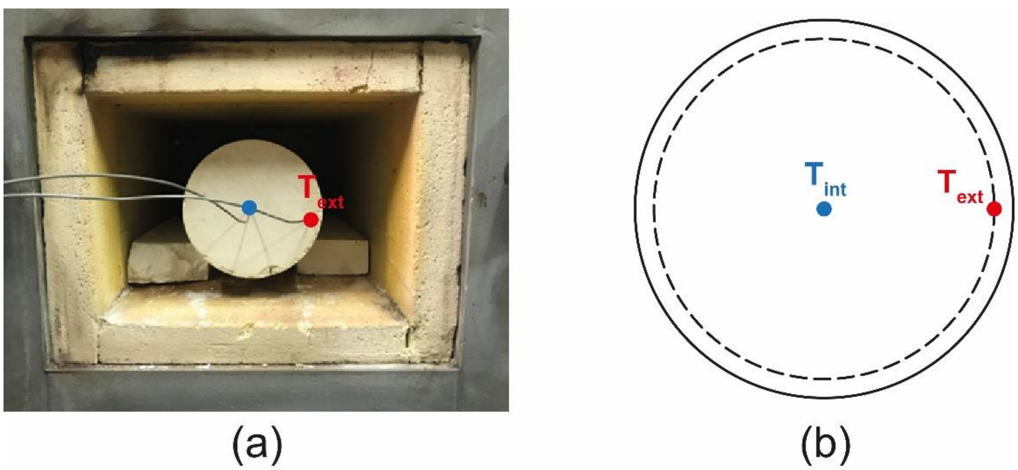

Figure 7. (a) Experimental set-up for diffusivity tests; (b) definition of the model, with actual boundary (continuous line) and fictitious boundary (dashed line).

Concerning the thermal properties used for the simulations, since the problem is governed by conduction only, the only governing parameter is the thermal diffusivity. The diffusivity relates the three parameters required for numerical thermal analyses, namely thermal conductivity λ, density ρ and specific heat c, through: $D = \lambda/(\rho \cdot c)$. Therefore, the simulations were carried out by using the thermal diffusivity measured in the tests (separately for the heating and the cooling phase). Assuming constant density (ρ = 2300 kg/m3) and specific heat (c = 1000 J/(kg·K)), this then allows determining an equivalent thermal conductivity, which is temperature-dependent., Note that this method could not be used in simulations involving boundary conditions by convection and radiation, because the thermal flux at the boundary would also be influenced by the value of the thermal conductivity (Robin-type boundary condition).

The results of the simulations are presented in Figure 8 and Figure 9 for the specimens S-D1 and S-D2, respectively. The two specimens were chosen because during the tests they exhibited a more regular behavior both in the heating and the cooling phase. The comparison shows good agreement between test results and numerical simulations.

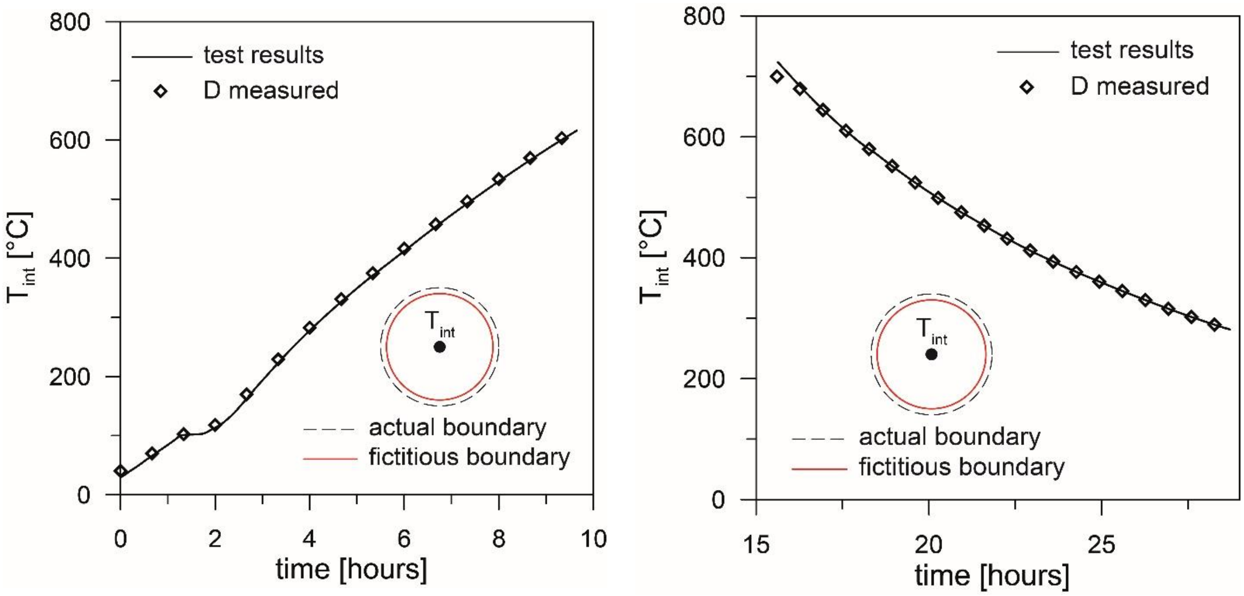

(a) (b)

Figure 8. S-D1: comparison between test results and numerical simulations for (a) heating and (b) cooling phase.

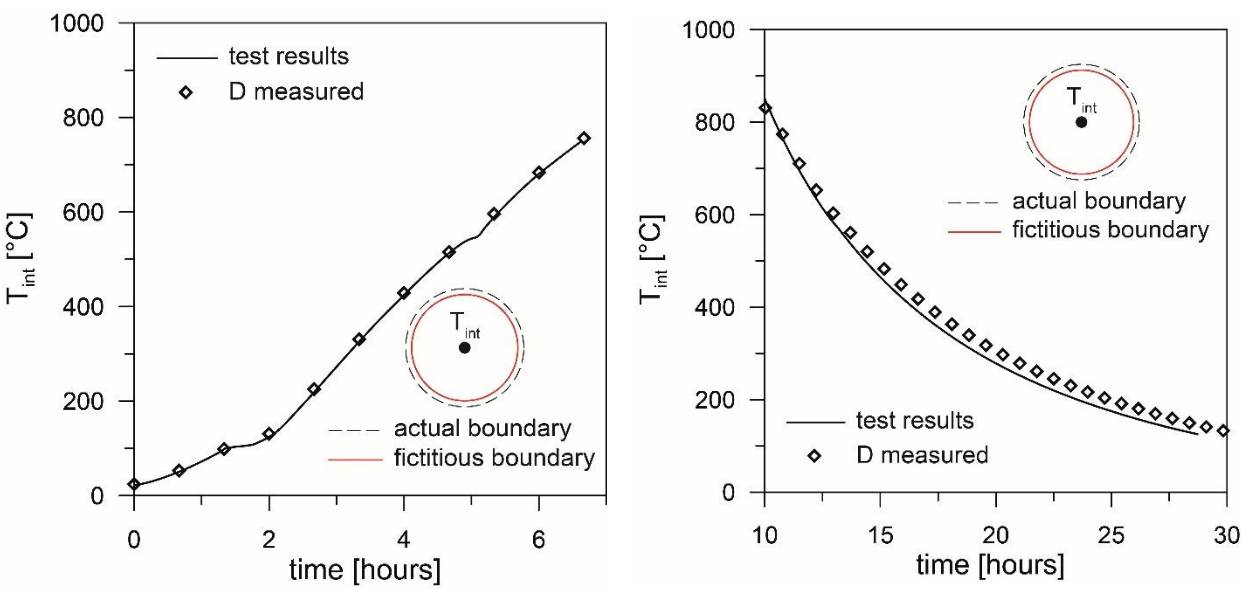

(a) (b)

Figure 9. S-D2: comparison between test results and numerical simulations for (a) heating and (b) cooling phase.

During the tests, there was a clear distinction between the heating and the cooling phase, because of the temperature imposed in the furnace and because of the uniformity of the thermal field inside the specimens. Yet, this is not always the case when dealing with reinforced concrete members exposed to fire, since (a) the thermal field is highly variable and (b) delayed heating usually takes place, thus leading to the onset of the cooling phase being different from point to point (i.e., more or less extended portions of a reinforced concrete member may undergo heating long after the onset of cooling along the boundary and in the superficial layers). To allow the possibility of performing numerical simulations including the irreversible behavior of concrete (as observed in the tests), in view of the structural applications presented in the following, a user subroutine was developed and used to simulate the whole thermal cycle on specimens S-D1 and S-D2. In the simulations, the thermal and physical properties were assumed according to the provisions of prEN1992-1-2. The results are shown in Figure 10, showing a very good agreement both in heating and in cooling.

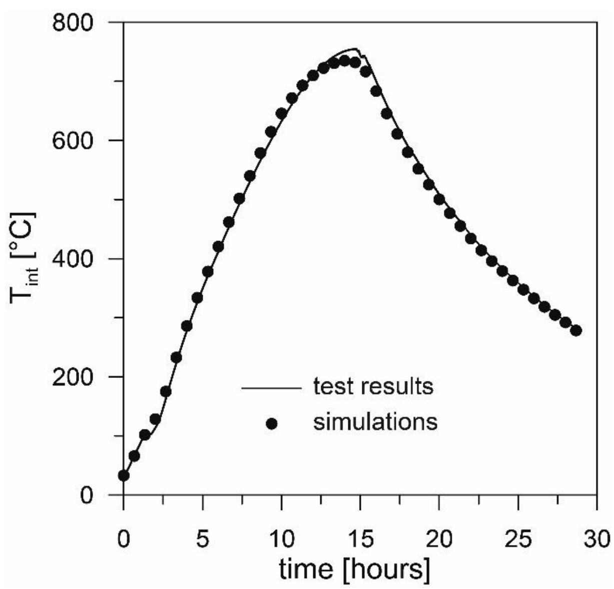

(a)

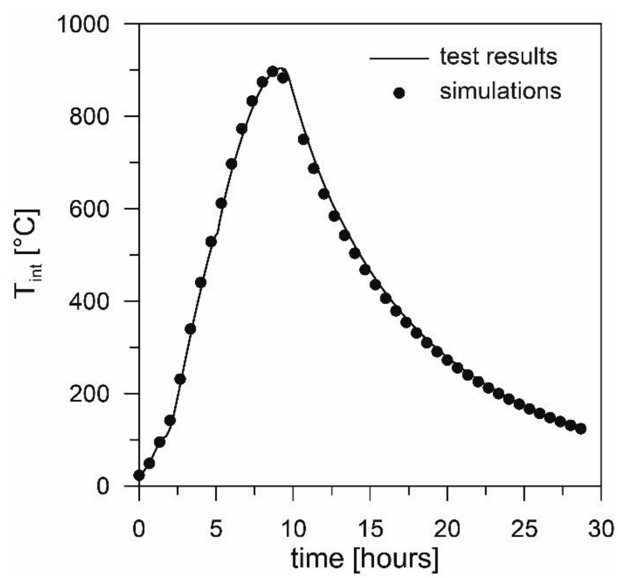

(b)

Figure 10. Comparison between test results and numerical simulations assuming the thermal and physical properties devised in prEN1992-1-2: (a) S-D1; and (b) S-D2.

2.3 Mechanical properties tests

The mechanical properties tests are devised to assess the behavior of concrete in a heating-cooling cycle. Therefore, the tests were planned as follows:

- For each test modality, two target temperatures are defined:
    - T_{max} = maximum temperature during the thermal cycle;
    - T_{test} = temperature at which the test is performed.

The temperatures selected for the different tests are the following, defined as a function of the maximum temperature reached during the thermal cycle:

- T_{max} = T_{test} = 20°C
- T_{max} = 200°C, T_{test} = 20 and 200°C
- T_{max} = 400°C, T_{test} = 20, 200 and 400°C
- T_{max} = 600°C, T_{test} = 20, 200, 400 and 600°C

For each test modality, two specimens are tested for repeatability, with one spare specimen available in case of large scatter. The heating rate is, in all cases, set to 1 °C/min in accordance with the RILEM guidelines on the basis of the diameter.

A summary of the test program is shown in Table 3. The tests at T_{test} = 20 °C (residual tests) have been completed for four different concrete batches, for a total of 32 mechanical tests (four temperatures T_{max}, four concrete batches, each repeated twice = $4 \times 4 \times 2 = 32$). As previously explained, the tests at high temperature were carried out on the first (S) and fourth concrete batch (C3), for a total of 24 mechanical tests (six combinations T_{max}-T_{test}, two concrete batches, each repeated twice = $6 \times 2 \times 2 = 24$).

Table 3. Test matrix for the mechanical tests, on one concrete batch.

		T_{max} [°C]			
		20	200	400	600
T_{test} [°C]	20	**2**	**2**	**2**	**2**
	200		**2**	**2**	**2**
	400		-	**2**	**2**
	600		-	-	**2**

Figure 11 shows the specimens inside the electric furnace prior to the thermal cycle at 600°C. Figure 12 shows the same specimens under the press after the thermal cycle. The rupture of the specimen was regular, with a pattern of cracks almost parallel to the axis of the specimens, with the exception of the highest grade concrete (C2, Figure 13), which exhibited a brittle failure at

200°C. Despite this failure, which is quite different from the others, the values of compressive strength measured are in line with those obtained on the other concretes (as will be shown later).

Figure 11. Specimens inside the electric furnace prior to the thermal cycle at 600°C.

(a) (b) (c) (d)

Figure 12. Specimens tested after the thermal cycle at 600°C: during compressive loading.

(a) (c) (d)

Figure 13. Specimens tested after the thermal cycle at 600°C: at failure.

After the thermal cycles and prior to testing, the specimens were weighed in order to check the mass loss. The results are shown in Figure 14. In all cases, the repeatability is quite good and the values are in agreement with the provisions of EN 1992-1-2, although the overall trend appears somewhat different in the case of the siliceous concrete.

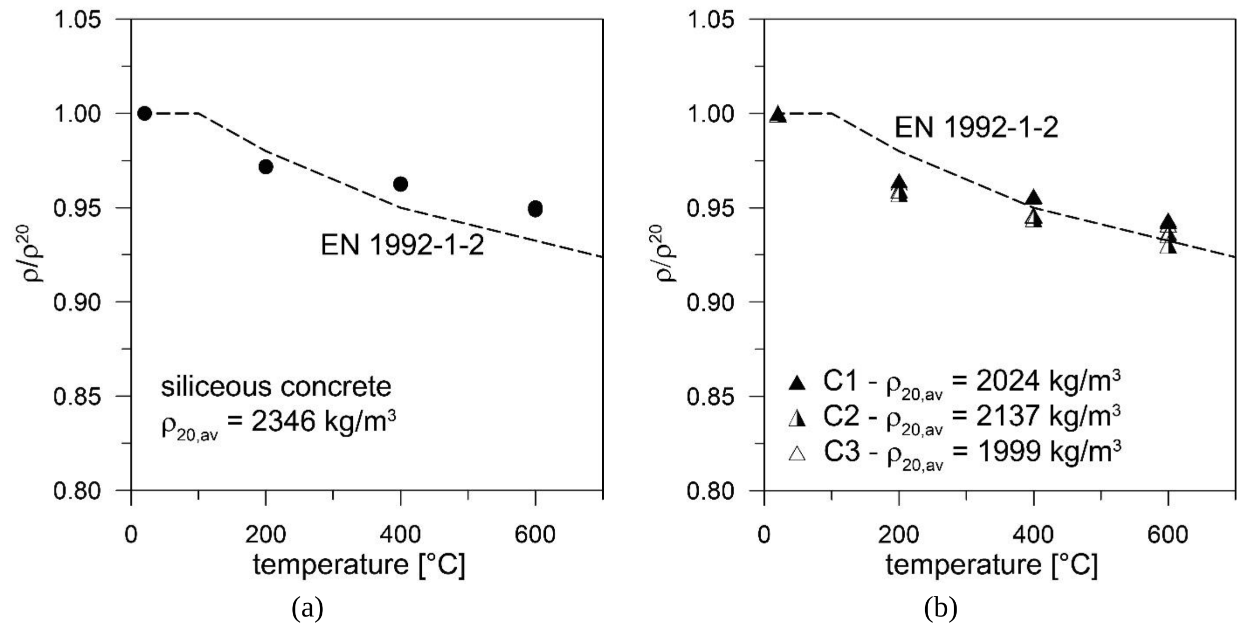

Figure 14. Mass loss for the siliceous (a) and calcareous concretes (b).

The test results obtained in the mechanical tests, for residual compressive strength at 20°C after heating, are shown in Figure 15. The siliceous concrete (Figure 15a) exhibits a decay of the compressive strength that is in agreement with the tentative provisions given in the draft of the new EN 1992-1-2 (the current version does not contain indications as regards residual values of the mechanical properties). As for the calcareous concrete, the measured decay is more pronounced than the corresponding values given in the cited standard (Figure 15b). The agreement improves if the experimental values are compared with the standard curves for siliceous concrete (Figure 15c). As a matter of fact, the three concretes C1-C3 contain mixed aggregate (siliceous + calcareous). As is visible in the diffusivity tests, with the downward spike at ≈ 575°C, the siliceous aggregates contained in the mix appears to have an influence on the behavior. Moreover, it is worth observing that the three concretes C1-C3 exhibit quite low values of density; this could also affect the behavior at high temperature, since porosity plays a more significant role with the loss of strength of the solid skeleton.

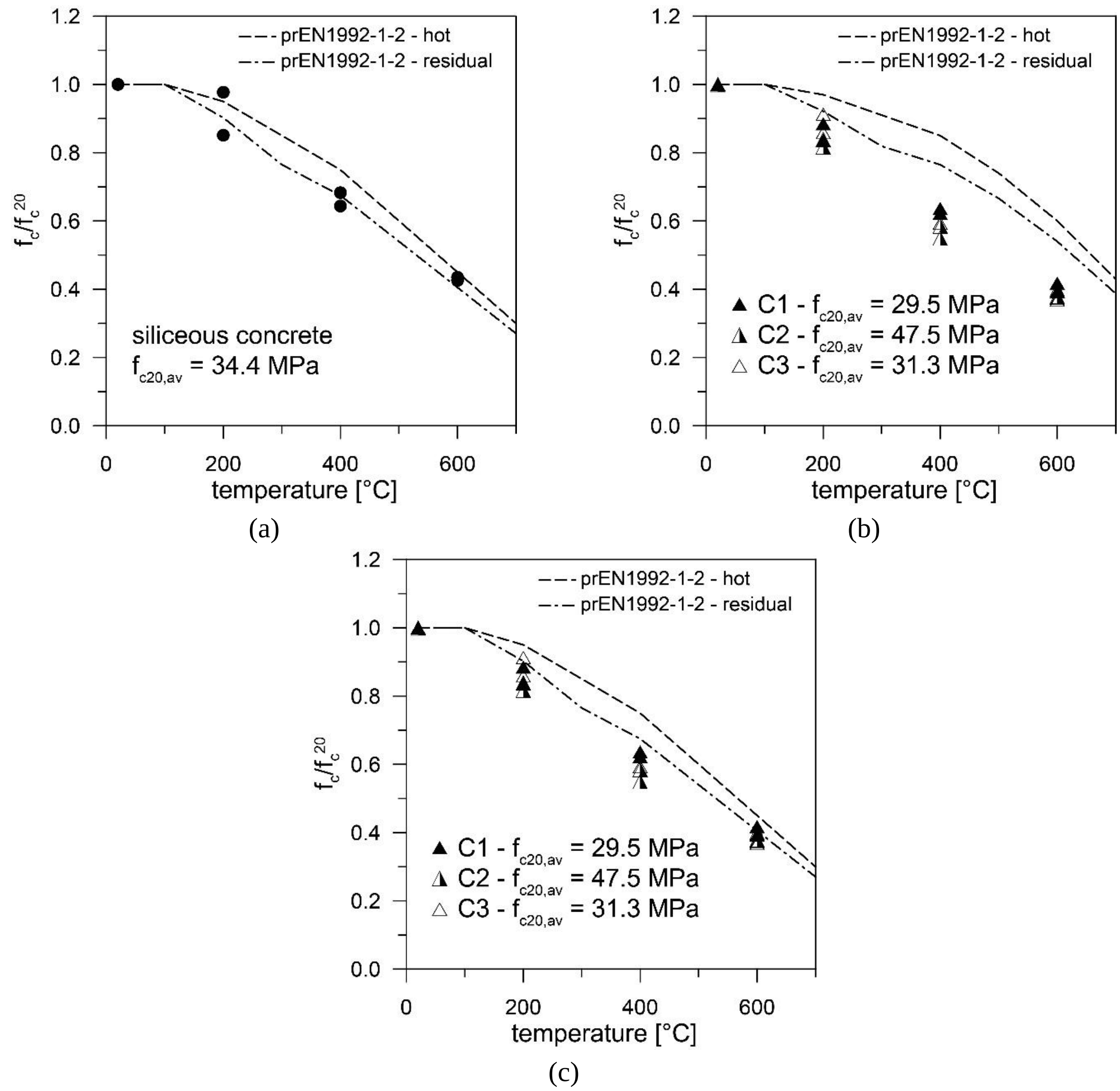

Figure 15. Results of the residual compressive tests. (a) Siliceous concrete. (b) Calcareous concretes. (c) Test results for the calcareous concretes, compared with the standard curves for siliceous concretes.

Table 4 summarizes the average values of the decay factors and corresponding coefficients of variation. The largest difference between the experimental values and values devised in prEN1992-1-2 was encountered at 400°C (0.62 versus 0.68), while there is good agreement at 200°C (0.87 vs 0.90) and 600°C (0.40 vs 0.41).

Table 4. Average values of the decay factors (f_c^T/f_c^{20}) and corresponding coefficients of variation for residual strength at 20 °C after exposure to elevated temperature T.

T [°C]	f_c^T/f_c^{20}	COV [%]
20	1.00	0.00
200	0.87	5.56
400	0.62	6.17
600	0.40	5.89

The results obtained in the mechanical tests at high temperature are shown in Figure 16 and Figure 17, for the first (S) and fourth (C3) concrete, respectively.

In the hot tests (T_{test} = T_{max}), the siliceous concrete (Figure 16a) exhibits a decay of the compressive strength which is close to the provisions given in the draft of the new EN 1992-1-2 (which are coincident with those given in [2]), although less pronounced beyond 400°C. Concerning the remaining tests (Figure 16b), with $T_{max} > T_{test}$, the tests characterized by T_{max} = 400°C are in quite good agreement with the provisions by EN 1992-1-2, while for T_{max} = 600°C the decay is clearly less pronounced with respect to EN 1992-1-2 (the dashed lines represent the continuous transition between hot tests, with T_{test} = T_{max}, and residual tests, with T_{test} = 20°C). In addition, it is worth noting that intermediate situations during the cooling from T_{max} to 20°C appear to be beneficial for the compressive strength for T_{max} = 600°C.

The same considerations also apply to concrete C3 (Figure 17). In the hot tests (Figure 17a), the decay is, on the whole, less pronounced in comparison to the provisions of EN 1992-1-2, especially for higher temperatures (T_{max} = T_{test} > 200°C). As concerns the tests with $T_{test} < T_{max}$, the trend observed in the siliceous concrete is confirmed, although the large scatter exhibited by the tests carried out at 400°C does not allow to draw final conclusions.

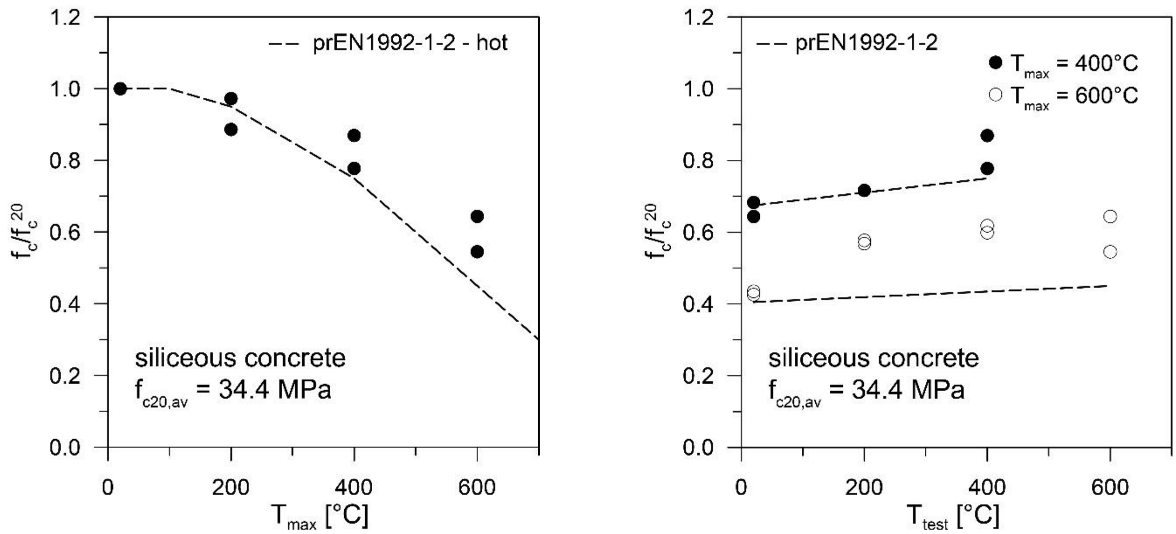

(a) (b)

Figure 16. Results of the high temperature tests carried out on siliceous concrete (S): (a) tests with $T_{test} = T_{max}$; (b) tests with $T_{test} < T_{max}$.

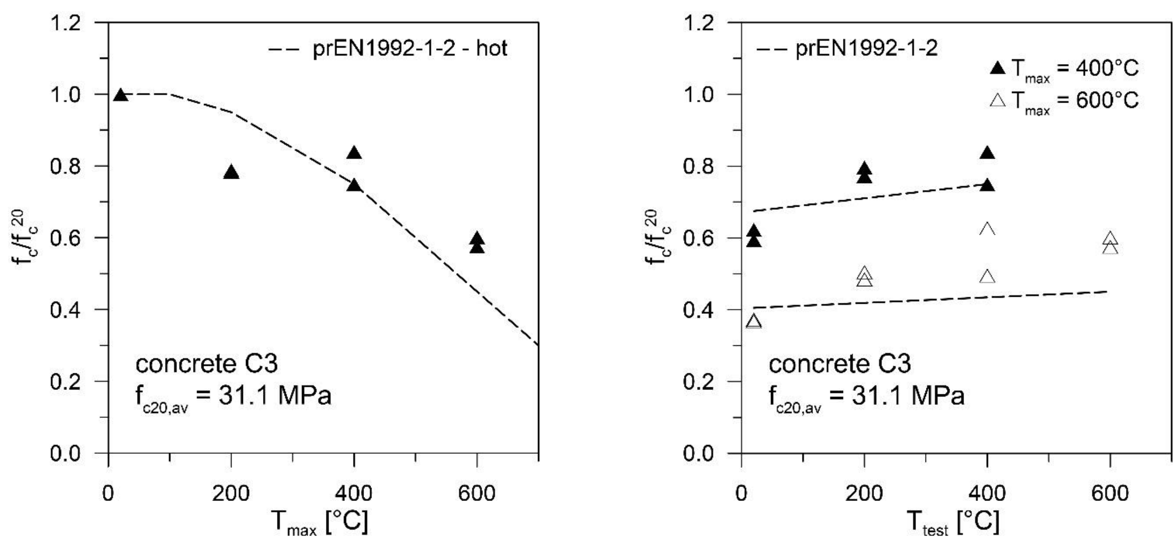

(a) (b)

Figure 17. Results of the high temperature tests carried out on calcareous concrete C3: (a) tests with $T_{test} = T_{max}$; (b) tests with $T_{test} < T_{max}$.

2.4 Material models and recommendations

The experimental data collected during the test campaign have been compared with the code provisions of EN 1992-1-2.

Based on the comparisons, the following conclusions can be drawn on the thermal properties of concrete during heating and cooling:

- Concerning the thermal diffusivity, in the heating phase the results appear to fall within the two boundary curves provided by the standard, although the agreement tends to worsen for temperatures above 500°C.
- Regardless of the behavior in the heating phase, the trend exhibited in the cooling phase clearly shows the irreversibility of the behavior. It is therefore reasonable to assume that, upon cooling, the diffusivity remains constant, and equal to the value attained at the maximum temperature reached during the thermal cycle.

The following conclusions can be drawn on the mechanical properties of concrete during heating and cooling:

- Concerning the residual mechanical tests (T_{test} = 20°C), the experiments have shown that the compressive strength of concrete is not recovered during cooling; in fact, an additional reduction in compressive strength occurs during cooling compared to the value at high temperature. The data for the residual strength of siliceous concrete exhibits a very good agreement with the tentative provisions given in prEN 1992-1-2. The calcareous concrete exhibits a more pronounced decay than the provisions, which could be due to the low density resulting from the presence of fibers in the mix. It is thus recommended to consider residual values for the compressive strength of concrete that are lower than the values at high temperatures.
- Concerning the mechanical tests at high temperature (T_{test} = T_{max}), the test results testify to the fact that the provisions of EN1992-1-2 are, on the whole, appropriately conservative.
- This research provided data for compressive strength of concrete during the cooling process, where the test temperature T_{test} was lower than the maximum reached temperature T_{max}, but still higher than 20°C. These data confirmed that cooling to 20°C leads to an additional reduction in strength, however, the reduction is not linear between the hot strength and the residual strength. At some intermediate temperatures during the cooling process, a temporary rebound in compressive strength was observed, with strength values higher than both the residual and hot values. Further research is needed to fully characterize the strength variation throughout the cooling process and, at the material level, elucidate the causes behind these observed variations.

3. Proposal of a Standardized Natural Fire Exposure

This task focuses on the fire exposure. The objective is to propose a standardized natural fire model for burnout resistance design. The model needs to encompass the different phases of real fires, yet at the same time be "standard" so it can be used efficiently to compare alternative structural solutions. In this task, simulations of fire development in building compartments are conducted. Experimental data on cooling rates is reviewed. In the end, this task results in the formulation of standardized natural fire curves for burnout resistance design.

3.1 The Eurocode EN1991-1-2 parametric fire model

The Eurocode EN1991-1-2 provides a parametric fire model to evaluate the time-temperature evolution in an enclosure during the heating and the cooling phases of a fire. Advantages of this model include the fact that it is well-known and widely used, implemented in a standard, and simple of utilization. Therefore, this model is well suited to build a standardized set of natural fire curves, which can be used for consistent comparison and analysis of burnout resistance.

According to the Eurocode parametric fire model, the time-temperature relationships during the heating and cooling phases are given by Eq. 3-1 and Eq. 3-2, respectively. The cooling down phase is linear, with a slope that depends on the duration of the heating phase.

$$\theta_g = 20 + 1325\left(1 - 0.324e^{-0.2t^*} - 0.204e^{-1.7t^*} - 0.472e^{-19t^*}\right) \; for\; t^* \leq \; t^*_{max} \quad \text{(Eq.3-1)}$$

$$\theta_g = \begin{cases} \theta_{g,max} - 625\;(t^* - t^*_{max} \cdot x) & for\; t^*_{max} \leq 0.5 \\ \theta_{g,max} - 250\;(3 - t^*_{max})(t^* - t^*_{max} \cdot x) & for\; 0.5 < t^*_{max} < 2 \\ \theta_{g,max} - 250\;(t^* - t^*_{max} \cdot x) & for\; t^*_{max} \geq 2 \end{cases} \quad \text{(Eq.3-2)}$$

In these equations, θ_g is the temperature in °C, $t^* = t \cdot \Gamma$ with t the time in hours and $\Gamma = (O/b)^2/(0.04/1160)^2$. The parameter O is the opening factor and b is the wall factor. The time of peak gas temperature is evaluated as: $t^*_{max} = t_{max} \cdot \Gamma$, with the time t_{max} calculated based on fuel-controlled or ventilation-controlled conditions in the compartment.

When the parameter Γ is set to unity, the heating phase approximates the ISO 834 temperature-time curve. This is convenient because it allows direct reference to a standard fire curve used to define the fire resistance rating. The standardized natural fire curve can then be based on the same heating curve as used for standard fire resistance, followed by a linear cooling. The temperature-time relationship of ISO 834 is given in Eq. 3-3 with the time *t* in min.

$$\theta_g = 20 + 345 log_{10}(8t + 1) \qquad with\; t\; in\; min \quad \text{(Eq.3-3)}$$

When setting Γ = 1, the parametric fire model depends on one parameter which is the time of maximum gas temperature t_{max}. In this work, this parameter is referred to as the Duration of Heating Phase (DHP). Figure 18 shows the time-temperature obtained with the parametric fire model Γ = 1, as a function of the DHP.

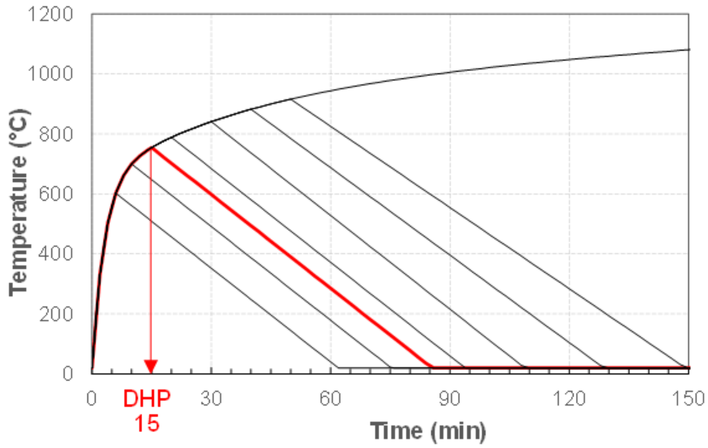

Figure 18. Standardized time-temperature curves for burnout resistance assessment.

Next, simulations of fire development in building compartments are conducted and experimental data are reviewed to assess a realistic range for the cooling rate in the fire model.

3.2 Modeling of enclosure fires with a zone model

Numerical simulations of fire development in compartments were conducted using the zone model software OZone [3]. Based on the fuel load and compartment characteristics, OZone computes the gas temperature in the compartment. OZone captures the heat and mass transfer between the inside of the compartment and the ambient external environment through vertical, horizontal and forced vents; the heat and mass produced by the fire; and the mass transfer from the lower to the upper layer by the fire plume. Table 5 gives the range of values considered for the input parameters in OZone.

Table 5. Values of parameters considered in the OZone simulations

Parameters	Range
Occupancy	Dwelling
Floor area (m^2)	9 – 16 – 25 – 36 – 64 – 100
Opening factors ($m^{1/2}$)	0.02 – 0.16
Height (m)	2.5 – 4
Thickness of gypsum board (mm)	0 – 25

As a sample of results, Figure 19 presents the compartment fire curves for an 8 m by 8 m by 3 m compartment with different opening factors. The opening factor influences significantly the peak temperature and the cooling rate.

The cooling phase of the fire curves is characterized by a fast cooling phase and a slow cooling phase, each of which can be idealized as linear. The rate of cooling of the fast cooling phase, in °C/min, is plotted against the opening factor in Figure 20. The cooling rate of the fast branch varies in a range of about 4-18 °C/min. The lowest cooling rates, i.e. the slowest cooling, occur for fires which are under-ventilated. The effects of the ceiling height, thickness of gypsum boards on the walls, and floor area on the cooling rate are similarly investigated, but the ventilation conditions have the predominant influence on the cooling rate.

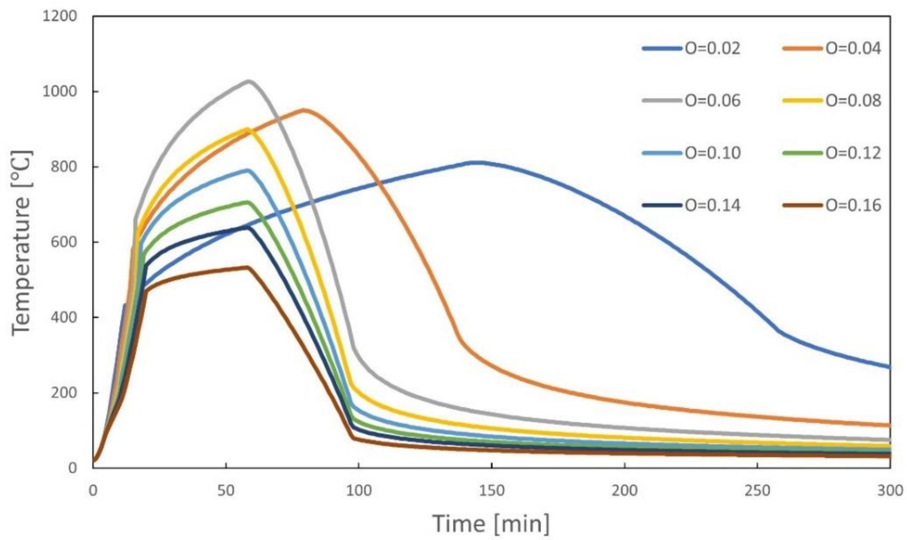

Figure 19. Fire curves computed by OZone for an 8 m by 8 m by 3 m compartment with different opening factors.

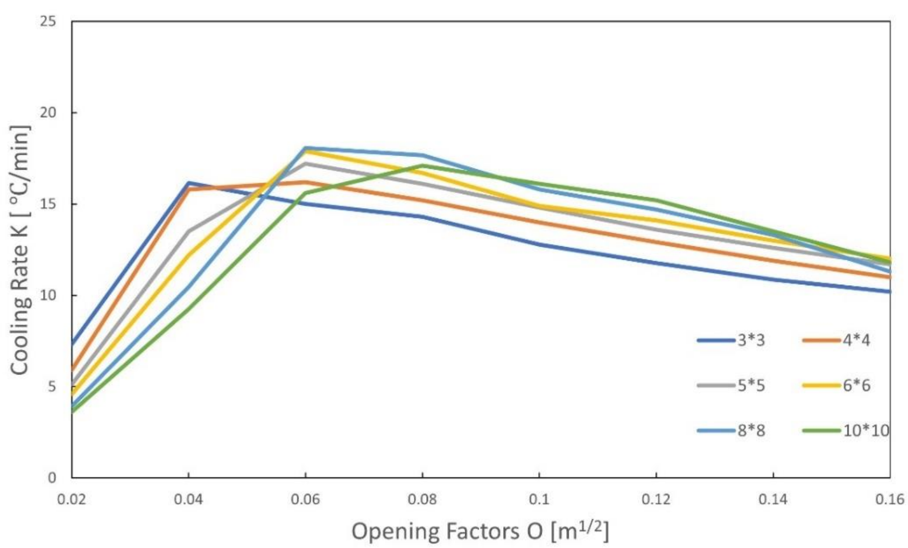

Figure 20. Fire cooling rate computed by OZone as a function of the opening factor.

3.3 Review of experimental fire curves in the Epernon test program

Several experimental test campaigns have been conducted in the last decades to measure the evolution of gas temperature in compartments during a fire. Here, test data from the recent Epernon test program (http://www.epernon-fire-tests.eu/) [4] is reviewed to gain further insights into typical cooling phases. Fire tests includes two different loaded structures, ceiling slabs made of cross-laminated timber (CLT) and ceiling slabs made of reinforced concrete. These two types of slabs were tested in compartment fire experiments with timber cribs as a fuel load. Different opening factors were tested. The dimension of the compartment was 6 m x 4 m in plan and 2.52 in height. The fire load during the compartment tests was 891 MJ/m² which is representative of the characteristic fire load for dwellings according to EN 1991-1-2 (Annex E) [5].

The temperature evolution in the compartments was recorded during the fire experiments. Table 6 gives the experimentally obtained cooling rates in the tests compartments. For the concrete experiments, the cooling rates vary from 7 °C/min to 28 °C/min.

Table 6. Experimental cooling rates during the Epernon fire tests.

	Cooling rate (°C/min)					
material	CLT			Concrete		
scenario	1	2	3	1	2	3
fast branch	40	18	6	28	26	16
slow branch	8	6	6	7	7	7
average rate	12	10	6	11	10	10

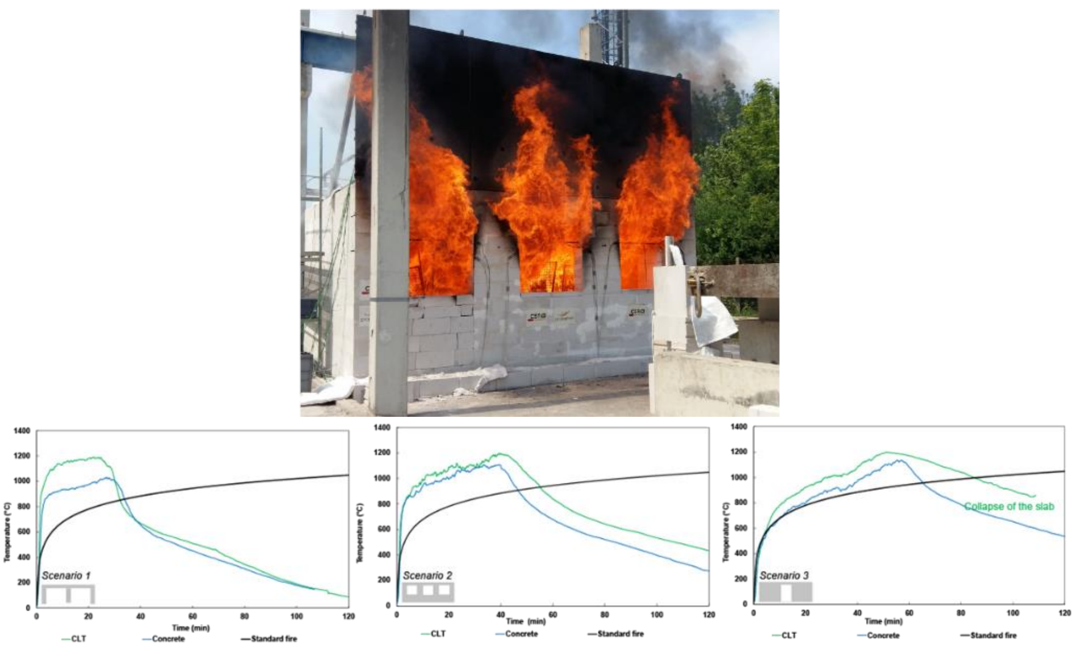

Figure 21. Picture from the Epernon test program and measured time-temperature curves. (source http://www.epernon-fire-tests.eu/)

3.4 Proposed fire model

The proposed standardized natural fire model for burnout resistance analysis has the following characteristics:

- It is based on the Eurocode EN1991-1-2 parametric fire model, a widely-used, standard fire model that includes a cooling down phase.
- The heating part of the fire follows the ISO 834 standard time-temperature curve used for fire resistance rating. This results from setting the parameter $\Gamma = 1$.
- The cooling part of the fire is linear, i.e. at a constant cooling rate. Based on the analyses above, it is proposed to consider a range of cooling rates from 2 °C/min to 20 °C/min.

The temperature-time relationship in the heating phase is given by Eq. 3-4, with t the time in hours and DHP the Duration of Heating Phase in hours. The temperature-time relationship in the cooling phase is given by Eq. 3-5, where K is the cooling rate in °C/hour.

$$\theta_g = 20 + 1325(1 - 0.324e^{-0.2t} - 0.204e^{-1.7t} - 0.472e^{-19t}) \qquad for\ t \leq DHP \qquad \text{(Eq.3-4)}$$

$$\theta_g = \theta_{g,max} - K\ (t - DHP) \qquad for\ t > DHP \qquad \text{(Eq.3-5)}$$

A sample of curves is plotted in Figure 22.

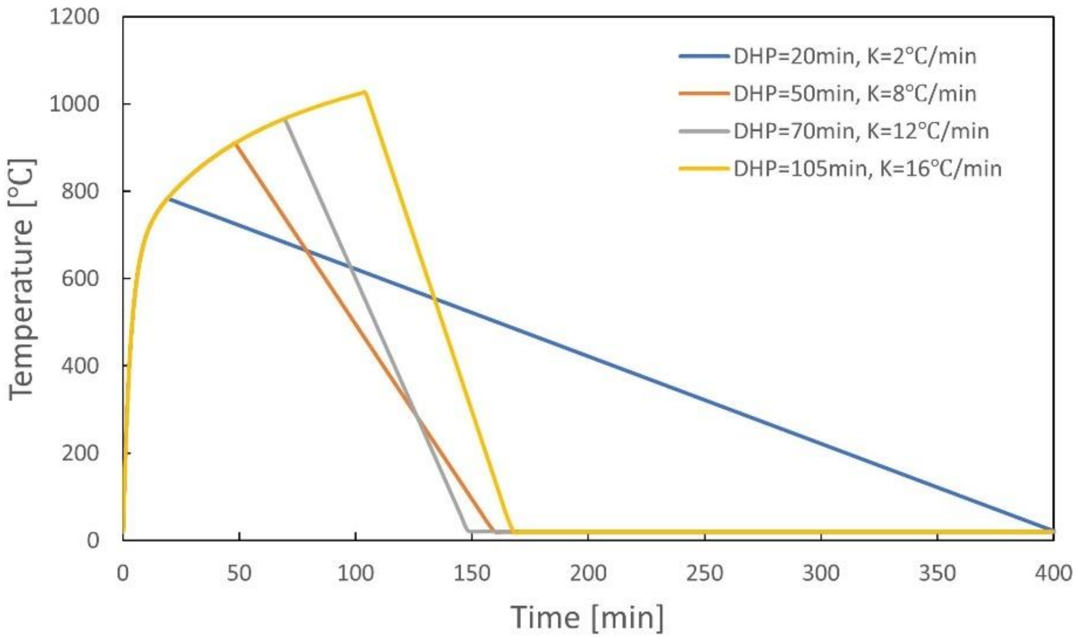

Figure 22. Examples of proposed standard natural fire curves.

4. Numerical Analysis of the Response of Concrete Members under Natural Fire

This task focuses on the response of structural members under fires with heating and cooling phase. The objective is to assess the burnout resistance of reinforced concrete members through thermal-structural analyses. The standardized natural fires previously defined are used as temperature-time boundary conditions in the thermal analyses. The analyses are conducted using the nonlinear finite element software SAFIR [6]. The task studies different prototypical RC members including columns, beams, and walls. The task results in a numerical database of standard fire resistance and burnout resistance for these members, including the effect of different cooling rates.

4.1 Method to evaluate the burnout resistance - DHP

The method to quantify the burnout resistance is based on the Duration of Heating Phase (DHP) indicator [7] as recently applied to reinforced concrete columns by Gernay [8]. It is briefly recalled here. Considering a set of standardized natural fire curves, the burnout resistance of a member is defined as the shortest fire that the member cannot survive. This shortest fire is standardized in terms of the DHP of the design natural fires (Figure 23). A member subjected to the DHP fire will fail, while it would survive a shorter fire (Figure 24).

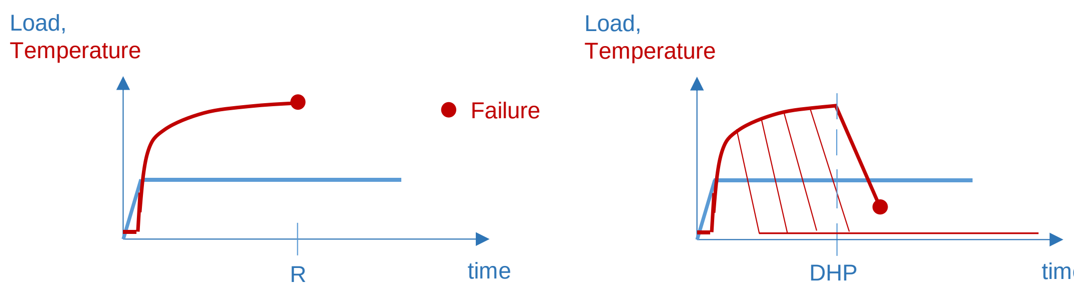

Figure 23. Concepts of fire resistance and burnout resistance based on Duration of Heating Phase.

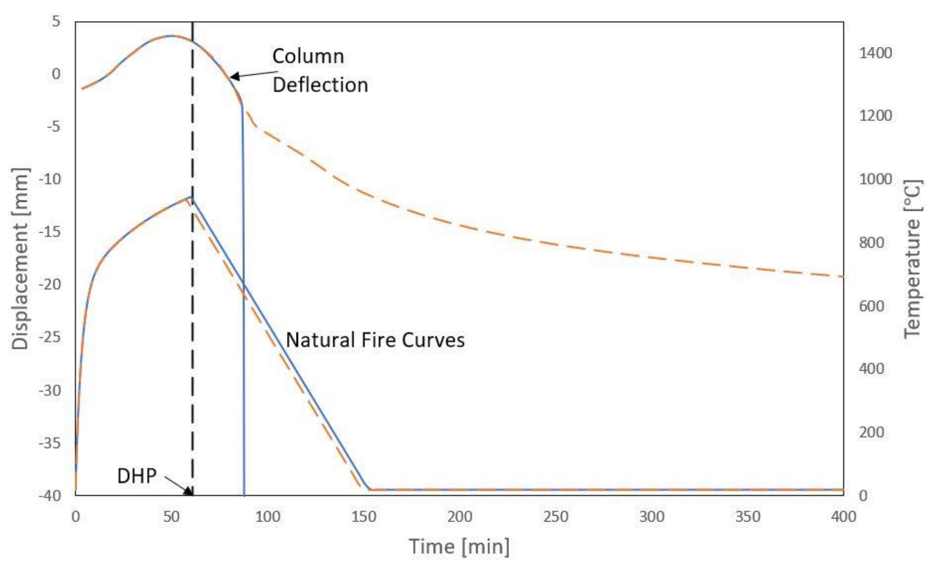

Figure 24. Behavior of a column under two standardized natural fire curves and the definition of burnout fire resistance (DHP). The slightly longer fire leads to structural collapse (during the cooling phase).

To evaluate the DHP, the member is subjected to fires of increasing duration of heating phase, until finding the fire that leads to loss of stability. This is an iterative process, easily implemented in a numerical framework (Figure 25). Simulations are run until the very end of the fire, when the temperature in the profiles are back to ambient, so that possible failures in cooling or thereafter are duly captured. The standard fire resistance is also computed to explore the relationship with the burnout resistance.

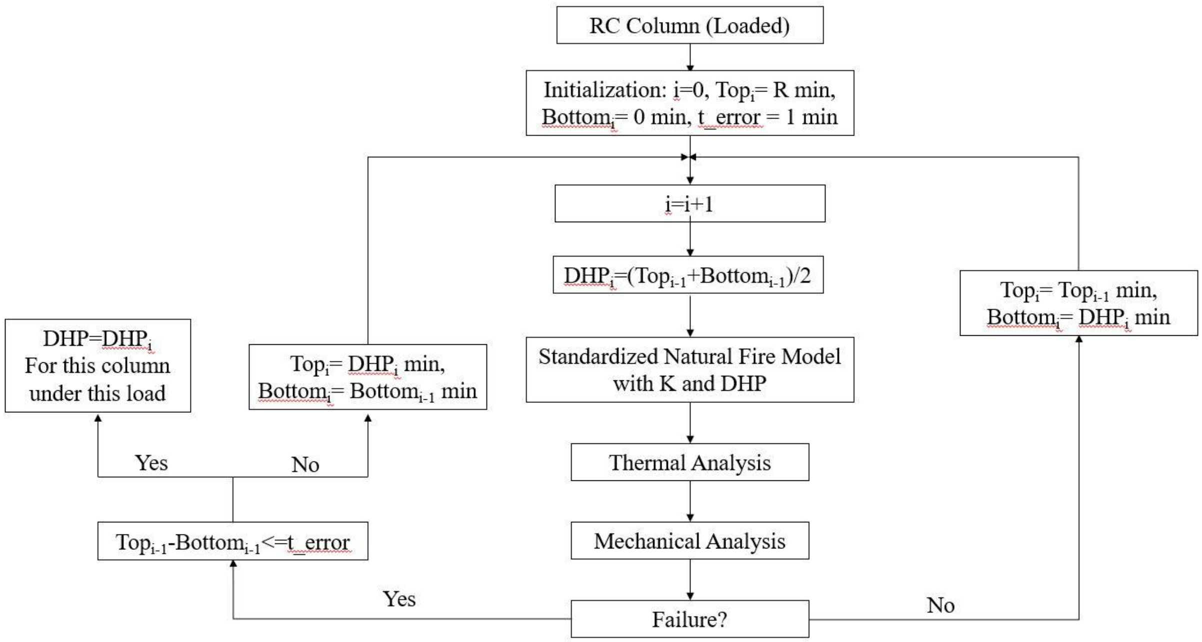

Figure 25. Numerical procedure to derive the DHP of a member.

4.2 Reinforced concrete columns

4.2.1 Prototypes

A database of 74 reinforced concrete columns is adopted. The 74 columns have been tested in standard furnace testing. 39 tests were conducted at the Technical University of Braunschweig in Germany (TUBr), 12 tests were conducted at the University of Ghent in Belgium (RUG), 4 tests were conducted at the University of Liege in Belgium (ULg), and 19 tests were conducted at the National Research Council in Canada (NRC). In each test, a loaded reinforced concrete column was exposed to a standard temperature-time curve on its four sides. The tests conducted in Europe used the ISO 834 thermal exposure while the tests conducted in Canada used the ASTM-E119 (ULC-S101), which is very similar.

The database has been described in details in a previous publication [8] and is not reproduced here for brevity. Parameters varied between the tests included the boundary conditions, length of the columns, cross sections, reinforcement ratio, material strengths, and magnitude and eccentricity of the load. The measured fire resistance varied from 31 min to 285 min for different specimens. The load level is an important factor; the fire resistance increases when the load decreases. The slenderness ratio also influences the fire resistance; the specimen with higher slenderness ratio generally leads to lower fire resistance.

4.2.2 Numerical model

The analysis of the behavior of the columns under fire is conducted using the finite element software SAFIR. The columns were previously analyzed under standard fire exposure on four sides to compare the numerical prediction with the test results [8]. Here, the columns are subjected to the standard natural fires described in Section 4, following the procedure of Figure 25 to derive their DHP.

First, thermal analyses are conducted to determine the transient temperature distribution in the cross-section of the columns under the different standard natural fires. The thermal analyses use 2D conductive solid elements. Convection and radiation with the hot gas is taken into account at the surface of the section. The discretization of the section of one of the columns is shown in Figure 26. The material models are in accordance with the Eurocode EN1992-1-2 [2]. The input properties used in the analyses are listed in Table 7. During the cooling phase, the thermal material properties are assumed as irreversible.

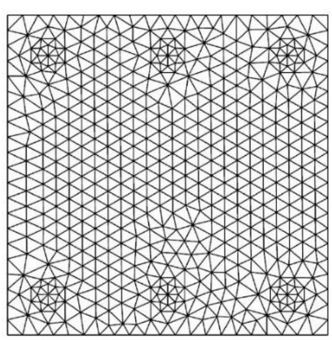

Figure 26. Discretization of the cross-section for the thermal analysis in SAFIR.

Then, mechanical analyses are conducted to evaluate the structural response of the columns subject to fire. The column is discretized using fiber-based beam finite elements. The transient temperature distribution in the section, pre-calculated from the thermal analysis, is taken into account at each time step. Large displacements are taken into account and buckling is captured. An initial imperfection consisting of a sine curve with a mid-height maximum deflection of L/1000 is introduced in the model. The material model SILCON_ETC (siliceous concrete) or CALCON_ETC (calcareous concrete) are used for the concrete. These models explicitly compute the transient creep strain. The material model STEELEC2EN is used for the reinforcement with a ductility limit at 0.05 strain. During the cooling phase, an additional strength degradation of 10% is adopted for concrete compressive strength, as compared to the strength value at the maximum reached temperature. The strain at peak stress and thermal properties are not recovered.

The axial load is applied at the top of the column within the first 20 s of the simulation and then maintained constant until failure, i.e. until the software is unable to find equilibrium for the structure (due to the thermal exposure). At that moment, an asymptote can be observed in the vertical displacement-time plot for the top node of the column, which indicates a 'physical' failure. Thus, in this numerical analysis, failure is defined as loss of structural integrity of the column, with no prescriptive failure criteria being applied. Both section failure and buckling failure are captured.

Table 7. Material properties used in the numerical model.

	Material Properties	Value
Concrete	Specific Mass [kg/m^3]	2400
	Moisture Content [kg/m^3]	72
	Convection Coeff. Hot [W/m^{2}K]	35
	Convection Coeff. Cold [W/m^{2}K]	4
	Emissivity	0.7
	Parameter of Conductivity	0
	Poisson Ratio	0.2
	Compressive Strength [MPa]	As per database
	Tension Strength [MPa]	As per database
Steel	Convection Coeff. Hot [W/m^{2}K]	35
	Convection Coeff. Cold [W/m^{2}K]	4
	Emissivity	0.7
	Young's Modulus [GPa]	210
	Poisson Ratio	0.3
	Yield Strength [MPa]	As per database
	Type	Hot-rolled Class A

4.2.3 Numerical results

For each of the 74 columns, the analysis yields the parameter DHP associated with the considered applied load and fire cooling rate. The DHP is the shortest duration of heating phase of the standard natural fire curve, for the given cooling rate, that leads to failure of the column. Thus, the DHP is correlated to the ability to survive a fire until full burnout; it divides the time domain between fires that are short enough to be survived and fires that will result in eventual collapse (for the considered column, fire model, and load level). The iterative procedure of Figure 25, including a series of thermal-mechanical analyses, is applied to each column and for 10 different values of the cooling rate *K*.

Figure 27 shows the relationship between the standard fire resistance R and the DHP computed with SAFIR for the 74 columns. These DHP refer to the standard natural fire with the cooling rate in accordance with the Eurocode parametric fire model (Eq. 3-2). By definition, the DHP is always shorter than R for a given column. The increase in (R – DHP) indicates a higher propensity to fail during or after the cooling phase for columns with longer fire resistance times.

The results for different cooling rates are plotted in Figure 28. Each curve represents one column. The curves relate the DHP, i.e. the minimum duration of heating phase of the standard natural fire resulting in a failure of the column, to the cooling rate of that natural fire *K*. The DHP decreases when *K* decreases because low cooling rates result in longer fires for a given DHP. Lower DHP (for a given R) indicate a higher propensity to fail during or after the cooling phase. Hence, the range of fires leading potentially to failure in cooling is greater when the cooling phase is longer.

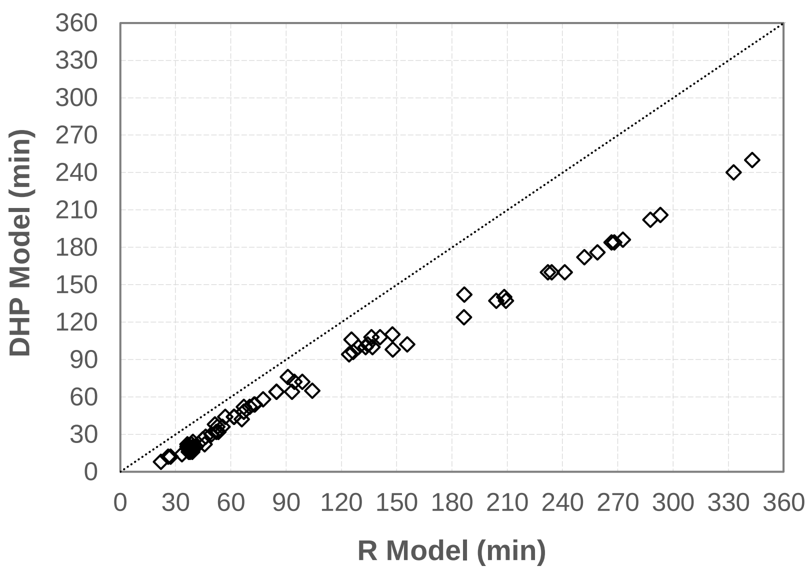

Figure 27. Relationship between R and DHP for the 74 columns (considering the standard natural fire with cooling rate in accordance with EN1991-1-2).

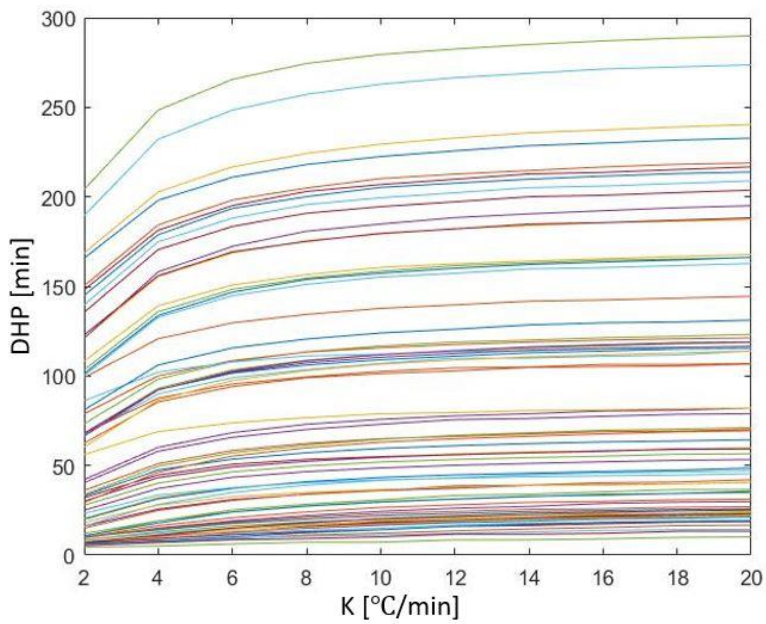

Figure 28. Results of the DHP evaluation for 74 columns, as a function of the cooling rate of the standard natural fire.

4.2.4 Discussion

The concept of time-equivalency has been explored by several researchers with the aim to relate different fire curves between them based on supposedly equivalent severity [9]. Here, several methods of equivalent fire severity are investigated. The objective is to understand whether the heating-cooling effects of the standard natural fire curves with different cooling rates can be related between them, and to an equivalent exposure time in the standard fire resistance test.

Equal area method

The concept was first proposed by Ingberg. The idea is to compare the area under time–temperature curves to measure equivalent fire severity. Two fires are considered to have equivalent severity if the areas under each curve, measured above a certain reference temperature, are equal. Even though this has little theoretical significance because the units of area are not meaningful, the equal area concept is a very simple method of comparing fires.

As an example, Figure 29 plots the relationship between the area above the 200°C threshold of the time-temperature curves resulting in failure and their cooling rates for the 74 columns. As can be seen, for a same effect (i.e. being the shortest duration of heating phase that leads to failure), fire models with a low cooling rate have a larger area than fire models with a high cooling rate. Similar plots are checked for various threshold temperatures between 100°C and 250°C, but the value of the reference temperature does not have an influence on such trend. It is noted that heat transfer from a fire to the surface of a structure is mostly by radiation. Since radiative heat transfer is proportional to the fourth power of the absolute temperature, heat transfer to the surface in a short hot fire may be larger than in a long cool fire. In any case, heat transfer is very nonlinear and the equal area concept fails to capture these effects.

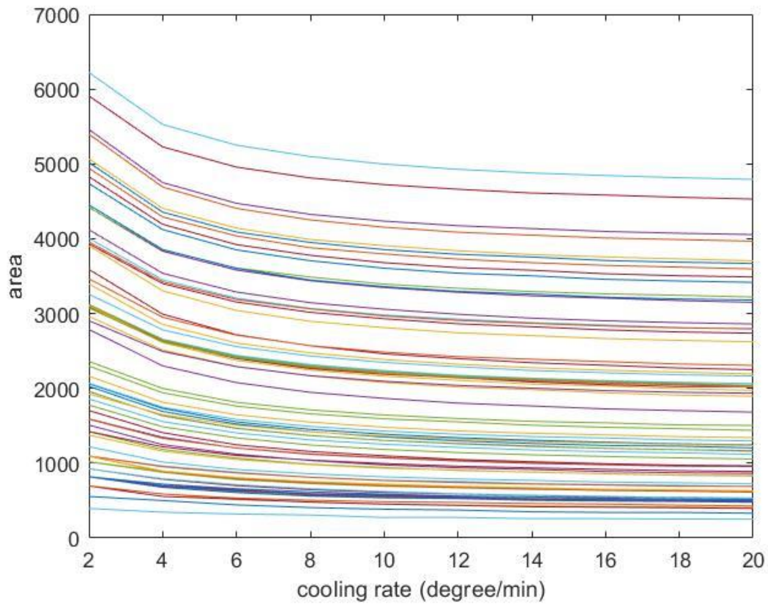

Figure 29. Shortest fire area resulting in failure as a function of the cooling rate of the standard natural fire.

<u>Maximum temperature in the section</u>

Another method, commonly used for steel design, is to define the equivalent fire severity as the time of exposure to the standard fire that would result in the same maximum temperature in the steel member as would occur in a complete burnout of the fire compartment, see Figure 30. This method is less appropriate to reinforced concrete members due to the large temperature gradients in the section. Nevertheless, it is sometimes applied to evaluate time equivalency for RC beams by using the rebar temperatures. For RC columns, since the concrete contribution to the ultimate strength is critical, it is unclear whether the nonlinear gradient in the section can be simplified into one meaningful temperature value. This idea is explored here by comparing the thermal profiles computed by finite element analysis for different fires having the same effect (i.e. different "DHP fires" obtained using different cooling rates for a same column).

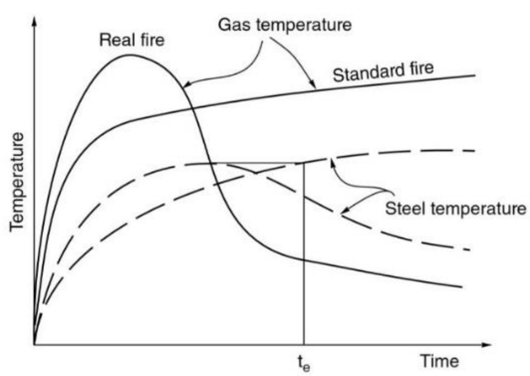

Figure 30. Concept of equivalent fire severity based on a critical temperature.

Figure 31 plots the temperature distribution at failure in the cross section of three different columns under fires with two different cooling rates. These pairs of temperature distributions have the same effect as they correspond to the time of failure of the columns. As can be seen, when a column is exposed to a slow-cooling fire, the temperature distribution is more uniform than under a fast-cooling fire. The temperature in the rebars is also different between these two situations. Unlike with a RC beam, the concrete part of a RC column has a large influence on the strength of the member. Therefore, looking only at a single maximum temperature, such as that of the rebar, is not applicable in the case of RC columns.

As a result, the DHP cannot be evaluated solely from a thermal analysis. It is necessary to run the structural analysis to determine whether the column would survive indefinitely the fire exposure. In Task 4, a simple design method to evaluate the DHP based on the fire resistance R and the cooling rate *K* will be proposed, using numerical results for calibration.

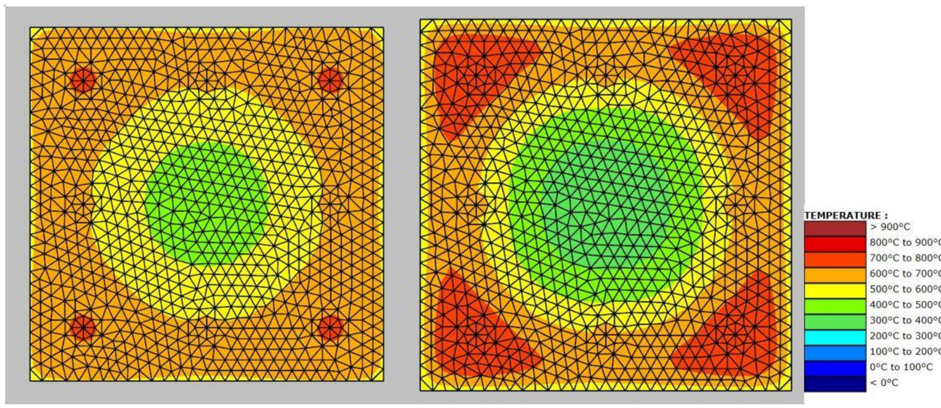

Test 69: temperature distribution comparison at failure for natural fires with K=2 (left) and K=8 (right)

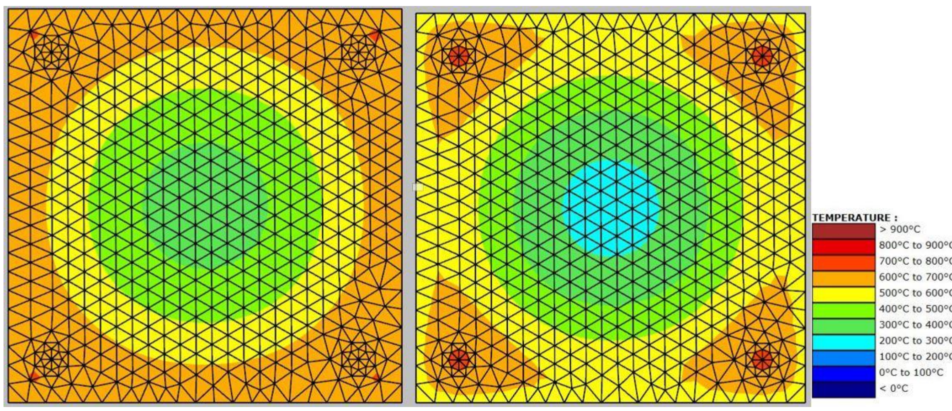

Test 44: temperature distribution comparison at failure for natural fires with K=2 (left) and K=8 (right)

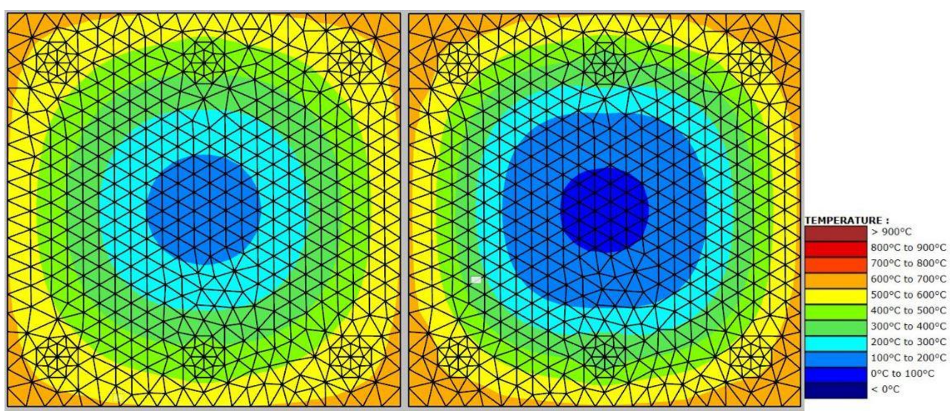

Test 1: temperature distribution comparison at failure for natural fires with K=2 (left) and K=8 (right)

Figure 31. Temperature distribution in cross-sections at time of failure under natural fires with different cooling rates.

4.3 Reinforced concrete beams

4.3.1 Prototypes

The beam tested by Sauca [10] is used as prototype to analyze the burnout resistance of reinforced concrete beams. The dimensions, loading conditions, and reinforcement layout are shown in Figure 32. The beam was tested under standard ISO fire until failure.

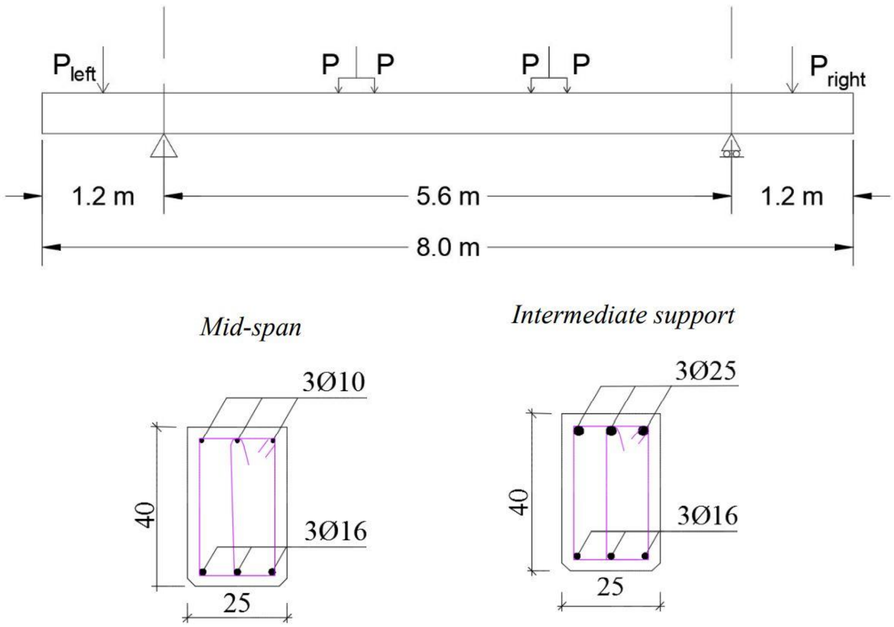

Figure 32. Dimensions and cross-section of the reference reinforced concrete beam.

Figure 33. Picture of the tested beam after failure (from Sauca [10]).

4.3.2 Numerical model

First, the thermal and mechanical behavior of the beam during the standard fire test is simulated to benchmark the numerical model. The numerical model is developed in SAFIR using the assumptions discussed in Section 5.2.2 and inputs from Table 8. The temperature computed by the numerical model agree with the measured temperatures during the test at the reinforcement location, see Figure 34.

The vertical displacement at mid-span is plotted in Figure 35. The failure occurred due to the formation of a plastic hinge at the mid-span. The agreement between the model and the test is good during the first 90 minutes, but failure occurred earlier in the test. The same observation was made by Sauca in her thesis which she attributed to some spalling of the beam during the experiment occurring between 85 min and 97 min. The numerical model, which does not capture spalling, predicts a failure at 125 min.

Table 8. Material properties used in the numerical model for the beam.

Material Properties		Value
Concrete (SILCON_ETC)	Specific Mass [kg/m^3]	2400
	Moisture Content [kg/m^3]	48
	Convection Coeff. Hot [W/m^{2}K]	25
	Convection Coeff. Cold [W/m^{2}K]	4
	Emissivity	0.7
	Parameter of Conductivity	0.5
	Poisson Ratio	0.2
	Compressive Strength [MPa]	48
	Tension Strength [MPa]	0
Steel (STEELEC3EN)	Convection Coeff. Hot [W/m^{2}K]	25
	Convection Coeff. Cold [W/m^{2}K]	4
	Emissivity	0.7
	Young's Modulus [GPa]	210
	Poisson Ratio	0.3
	Yield Strength [MPa]	500
	Type	Cold formed class B

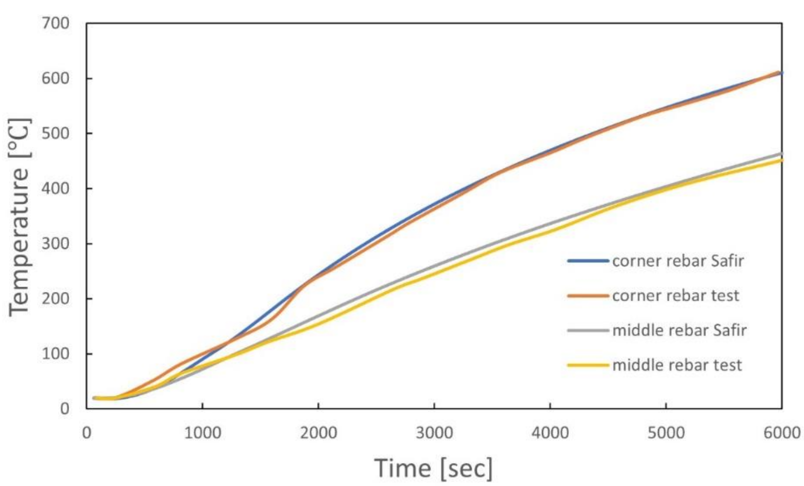

Figure 34. Comparison between computed and measured temperatures in the tested RC beam.

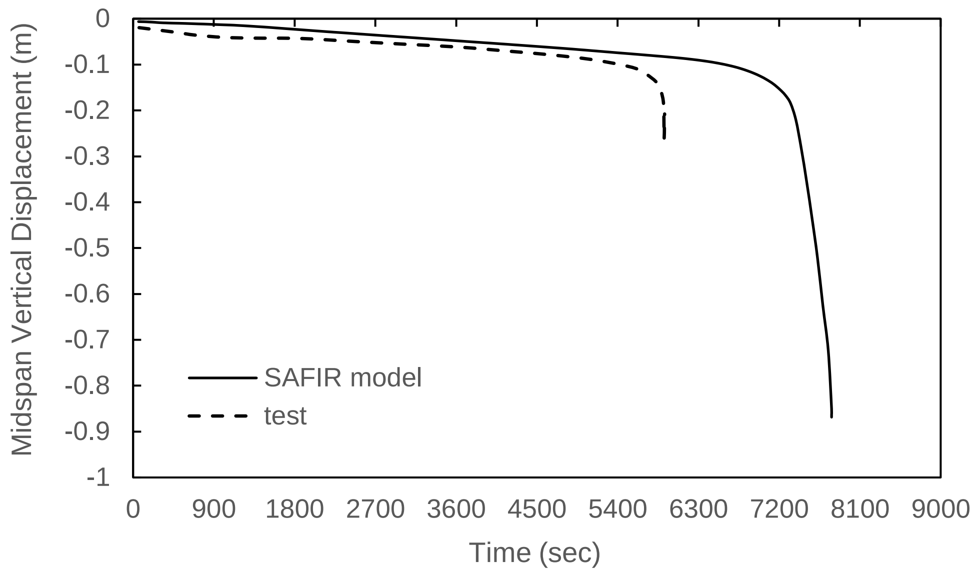

Figure 35. Comparison between computed and measured displacements of the tested RC beam.

4.3.3 Numerical results

The prototype beam was then subjected to the standard natural fires to evaluate the burnout resistance. The numerical procedure of Figure 25 was applied. Different loading levels were considered. The cooling rate *K* of the standard natural fires was varied from 2 °C/min to 20 °C/min. The results are given in Table 9. The results reveal a significant effect of the cooling rate on the susceptibility to delayed failure.

Figure 36 shows the relationship between the standard fire resistance R and the DHP computed with SAFIR for the beams. The values of DHP plotted in Figure 36 refer to the standard natural fire with the cooling rate following the Eurocode parametric fire model (Eq. 3-2). By definition, the DHP is always shorter than R for a given column. The value of (R – DHP) indicates the propensity to fail during or after the cooling phase for beams. This value is approximately constant, i.e., independent of the fire resistance R.

The DHPs of beams with different cooling rates are plotted in Figure 37. Each curve represents one case in Table 9. The curves relate the DHP to the cooling rate *K* of that natural fire. The results for the beams show the same trend as those for the columns in Section 5.2. The DHP increases when *K* increases because higher cooling rates result in shorter fires for a given DHP. A lower DHP (for a given R) indicate a higher propensity to fail during or after the cooling phase. The range of fires leading to failure in cooling is greater when the cooling phase is longer.

Table 9. Burnout resistance (DHP) of the beam as a function of loading and cooling rates.

Case	P right, P left (N)	P (N)	R (min)	K (℃/min)	DHP (min)
1	67,500	18,400	125	2	76
				4	96
				6	103
				8	107
				10	110
				12	111
				14	112
				16	114
				18	114
				20	115
2	135,000	37,000	93	2	39
				4	57
				6	65
				8	70
				10	72
				12	75
				14	77
				16	77
				18	78
				20	78
3	150,000	38,000	98	2	44
				4	63
				6	70
				8	75
				10	78
				12	79
				14	81
				16	82
				18	82
				20	84
4	0	12,000	109	2	54
				4	73
				6	81
				8	87
				10	88
				12	90
				14	92
				16	94
				18	94
				20	95
5	97,500	25,400	118	2	65
				4	84
				6	91
				8	95
				10	99
				12	99
				14	101
				16	102
				18	103
				20	103

6	0.	9500	120	2	67
				4	86
				6	94
				8	99
				10	100
				12	103
				14	104
				16	105
				18	105
				20	105
7	0	7500	134	2	77
				4	97
				6	105
				8	110
				10	113
				12	114
				14	116
				16	117
				18	117
				20	119
8	37,500	10,000	184	2	122
				4	149
				6	158
				8	162
				10	165
				12	167
				14	168
				16	169
				18	169
				20	170
9	30,000	7500	265	2	231
				4	243
				6	247
				8	250
				10	252
				12	252
				14	252
				16	253
				18	254
				20	254

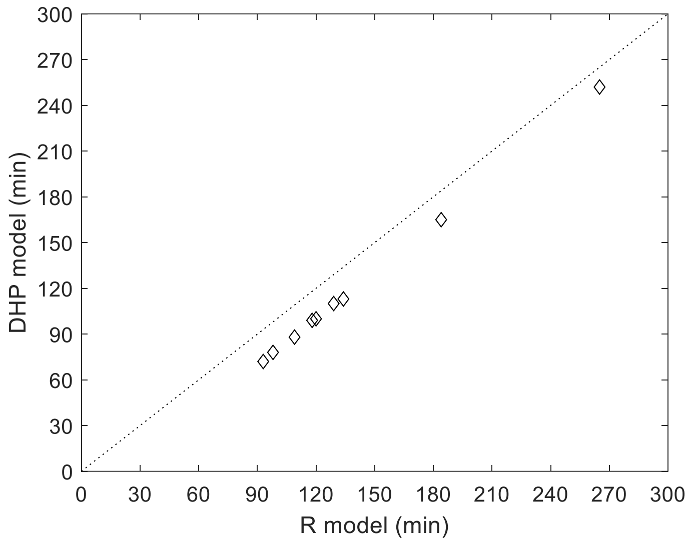

Figure 36. Relationship between R and DHP for the beams (considering the standard natural fire with a cooling rate following the Eurocode parametric fire).

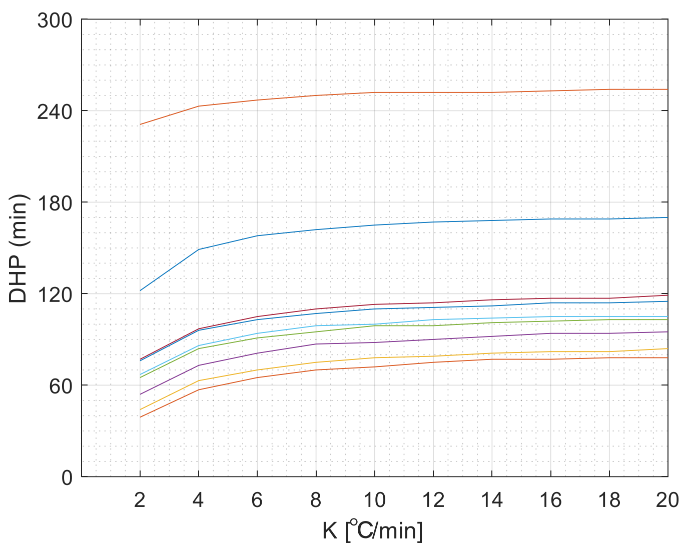

Figure 37. Results of the DHP evaluation for the beams, as a function of the cooling rate of the standard natural fire.

4.3.4 Simplified approach

In the case of statically determinate members, such as simply supported beams and one-way slabs, EN 1992-1-2 (Annex E) allows to evaluate the reduction of the loadbearing capacity in positive bending by simply considering the temperature reduction of the mechanical properties of the reinforcement in the critical section (i.e., at midspan). This simple and straightforward approach is justified by the usual design procedures, which imply that reinforced concrete members are designed with light reinforcement (to attain a ductile behavior at impending failure). Moreover, in a typical fire situation (where the fire is at the soffit of beams and slabs) the bottom rebars are significantly heated and therefore are primarily responsible for the reduction of the bearing capacity (a minor role is played by the reduction of concrete properties). It is worth noting, however, that in its current formulation, the validity of the method is limited to the case of fires without a decay phase. In the most recent draft of the new Eurocode 2 (prEN 1992-1-2) this method will replace the well-known simplified analysis based on a reduced section, in the case of beams.

The approach was applied to Cases 1-6 as presented in Table 9 with the objective of checking its applicability to the cases of natural fires. To this end, thermal analyses were carried out on the beam section (Figure 32) subjected to the natural fires determined by the previously presented iterative analyses, i.e., fires characterized by a given value of DHP and the corresponding cooling rate *K*. The results of the thermal analyses allow to determine the temperature T_i as a function of time for each rebar at the bottom of the section. From this temperature T_i, one can evaluate the corresponding strength retention factor k_{si} for the rebars. The strength retention curve for cold worked steel from EN 1992-1-2 is used. The reduction of the loadbearing capacity is then identified with the average value k_{av} of the k_{si} values, worked out on the basis of the maximum temperature reached by each rebar during the whole fire. This conservative assumption is justified by the fact that the maximum temperature in the lower reinforcement occurs at approximately the same time; besides as this maximum temperature exceeds 500 °C (in most of the cases), irreversibility of steel thermal damage is expected. Note that this way of performing the calculations reflects a typical design-oriented (or assessment-oriented) procedure, where the DHP is an input data, rather than the result of an iterative procedure, as in the case of the advanced calculations described in the previous sections.

The results of the analyses are shown in Figure 38. The figure plots the average retention factor of the lower reinforcement experienced under the DHP fires with different cooling rates. These retention factors represent the minimum strength retained by the lower reinforcement under natural fires that led to structural collapse. The figure also plots the load ratio applied on the beams as horizontal dashed curves. The simplified approach proves to yield results that are on the safe side in all cases, considering that the reduction of the loadbearing capacity (represented by the symbols) as a function of the cooling rate is lower than the load ratio (represented by the dashed lines), thus implying that the simplified approach adopted would predict the member to fail under the considered fires.

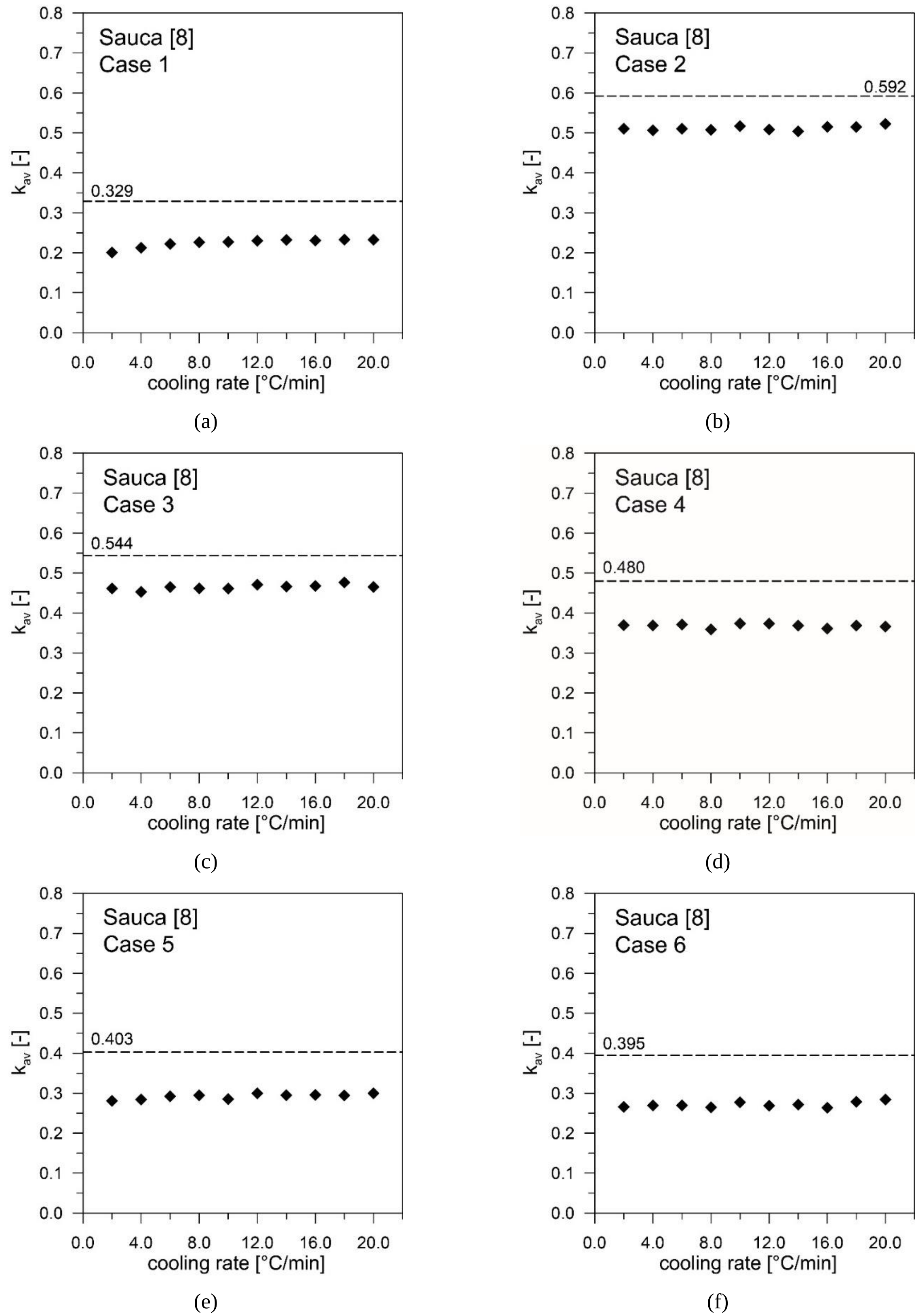

Figure 38. Results of the simplified approach based on minimum strength retained in the lower reinforcement for the beam: (a) Case 1. (b) Case 2. (c) Case 3. (d) Case 4. (e) Case 5. (f) Case 6.

4.3.5 Discussion

The capacity in the fire situation of reinforced concrete beams largely depends on the temperature in the reinforcement bars. The concept of equivalent fire severity based on lower rebar temperature is likely to apply better to beams than columns. Therefore, the thermal results are further analyzed here. The temperature distribution in the section at the time of failure is compared for different cooling rates.

Figure 39 plots the temperature distribution at failure in the cross-section of the beam under fires with two different cooling rates, *i.e.*, K = 2 and K = 10 °C/min. The beams from Test 3 and Test 6 are presented; the difference between the two tests lies in the loading ratio and hence in the DHP and the time of failure. For each test, the pairs of temperature distributions that are plotted have the same effect as they correspond to the time of failure of the beams. As can be seen, when a beam is exposed to a slow-cooling fire (K = 2 °C/min), the temperature distribution is more uniform than under a faster-cooling fire (K = 10 °C/min). The difference is more pronounced for the concrete core of the section than for the lower reinforcement, which is close to the exposed surface. The temperature of rebar at failure in a beam with a slow cooling rate is only slightly lower than that with a fast cooling rate. Therefore, considering the maximum rebar temperature as a failure criterion is an approximation for RC beams failing in cooling.

Concerning the applicability of the simplified approach proposed in EN 1992-1-2 (Annex E), the results obtained in six of the cases summarized in Table 9 testify to the safeness of the approach.

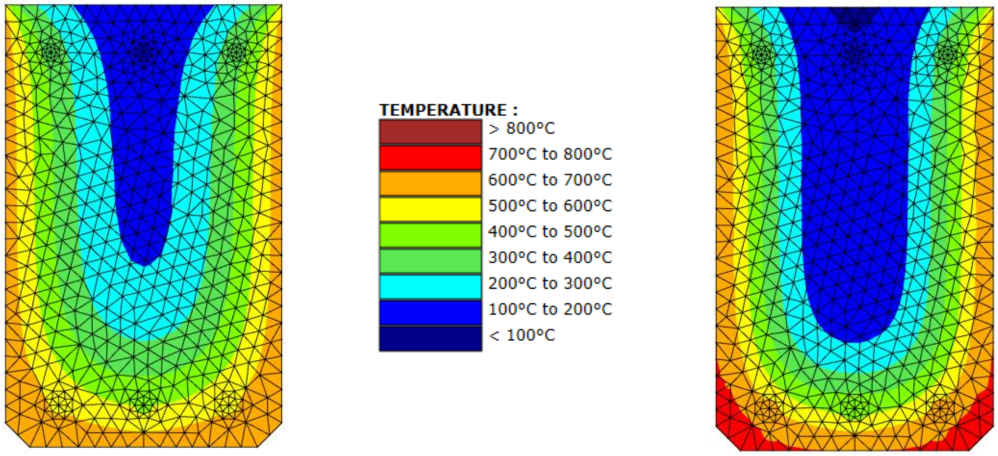

K = 2 °C/min K = 10 °C/min

Test 3

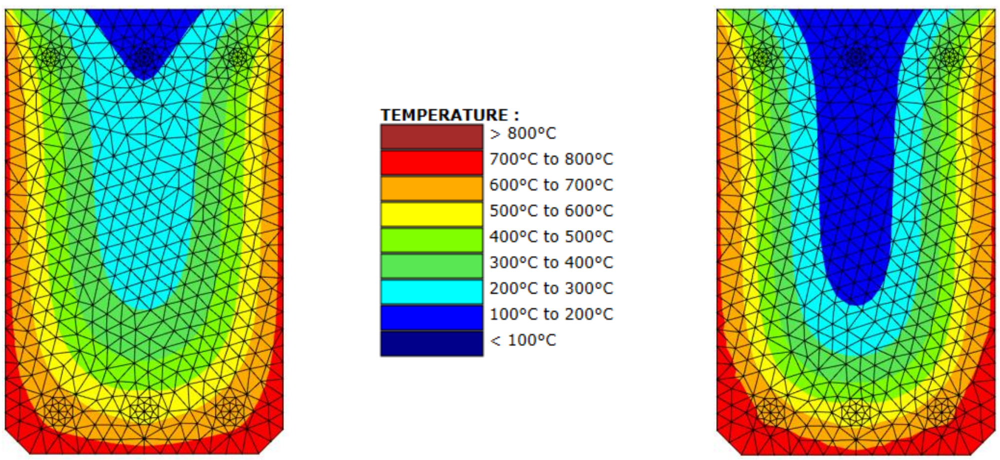

K = 2 °C/min K = 10 °C/min

Test 6

Figure 39. Comparison of the temperature distribution in the mid-span cross-section at failure for natural fires with different cooling rates K.

4.4 Reinforced concrete walls

4.4.1 Prototypes

The high-rise RC wall tested by D. T. Pham et al. [11] in 2021 (Figure 40) are used as prototype to benchmark the numerical model for evaluating RC walls under natural fires. The test is designed to investigate the behavior of a slender wall with a very large height/thickness ratio under standard fire exposure. The tested wall is 2.6 m-wide, 8.4 m-high and 0.15 m-thick. The height/thickness ratio equals 56. It is heated by the ISO 834 fire on one side for 90 minutes and only subjected to the thermal load and its self-weight. In terms of the boundary conditions, the wall is hinged at both ends while the top support allows free vertical movement. The concrete has a compressive strength of 36.1 MPa and tensile strength of 2.75 MPa. The wall was reinforced with two symmetrical layers of 9 mm diameter hot rolled steel reinforcing bars of yield stress f_y = 480 MPa and Young's modulus E_s = 210 GPa, with a spacing of 100 mm. The steel bars were arranged in two orthogonal arrays and placed with 25 mm of concrete cover at both the top and the bottom parts of the wall thickness. Figure 40 shows the details of the reinforcements layout and the test setup.

Figure 40. Details of the test RC wall (a. rebar layout, b. test setup).

4.4.2 Numerical model

The numerical model is verified by comparing the predicted numerical solution with the measured test results. Shell elements are used for the structural analysis at elevated temperature. The shell element in SAFIR is a four-node quadrilateral element with constant thickness. There are four Gauss integration points on the surface of the shell element. There are also integration points distributed across the depth of the shell at the positions of the surface integration points. The number of Gauss integration points across the thickness is defined by the user. This type of element is usually used to model structures where one dimension, thickness, is significantly smaller than the other two dimensions. It is thus suitable for walls and slabs. For instance, Lim L et al. [12] used shell elements to model two-way reinforced concrete slabs in the fire in SAFIR. The numerical results showed good agreement with the tests results, verifying the shell elements for these types of applications.

The material properties used to model the high-rise wall are summarized in Table 10. The concrete model is taken as 'SILCOETC2D' for structural analysis. This is a plastic-damage model [13] with explicit transient creep formulation [14]. 'STEELEC2EN' is used for the reinforcement and the material is assumed as hot-rolled class A.

Table 10. Summary of material properties for the test wall simulation.

	Material Properties	Value
Concrete	Specific Mass [kg/m^3]	2400
	Moisture Content [kg/m^3]	72
	Convection Coeff. Hot [W/m^{2}K]	25
	Convection Coeff. Cold [W/m^{2}K]	4
	Relative Emissivity	0.7
	Parameter of Thermal Conductivity	0 (lower limit)
	Poisson Ratio	0.2
	Compressive Strength [MPa]	36.1
	Tension Strength [MPa]	2.75
	Strain at Peak Stress	0.0031
	Comp. Damage Peak Stress	0.35
	Tension Ductility [N/m^2]	200
Steel	Convection Coeff. Hot [W/m^{2}K]	25
	Convection Coeff. Cold [W/m^{2}K]	4
	Relative Emissivity	0.7
	Young's Modulus [GPa]	210
	Poisson Ratio	0.3
	Yield Strength [MPa]	480
	Type	Hot-rolled class A

The thermal analysis is performed by discretizing the cross-section into 20 elements along the depth of the wall to capture the across-thickness temperature gradients. Figure 41 shows the thermal analysis model, with the temperature distribution after 90 minutes of ISO fire exposure.

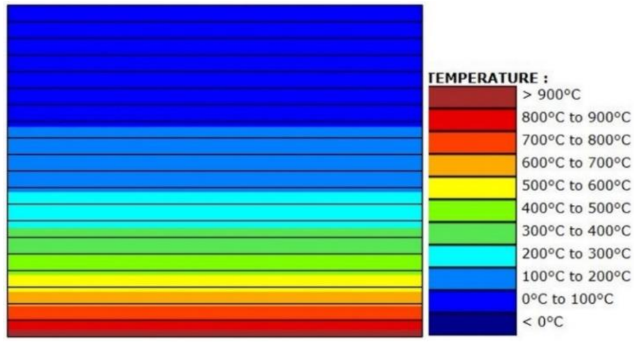

Figure 41. Discretization of the test wall for thermal analysis and temperature distribution at 90 min.

The temperature distribution at different times is plotted in Figure 42 and compared with the measurements. Good agreement can be observed between the numerical results and the test results. It is obvious that the temperature at various depths of concrete, as well as in rebars, increases with fire exposure time. As expected, sthe predicted temperature decreases with increasing distance from the fire exposed side. This comparison validates the thermal model.

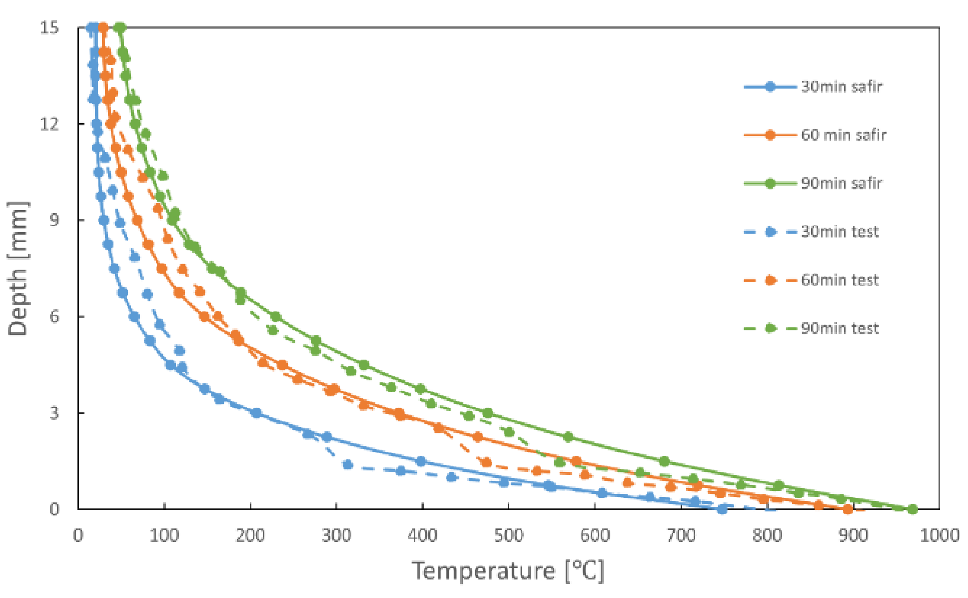

Figure 42. Comparison between test results and numerical results for thermal analysis.

The 3D shell element model for structural analysis is shown in Figure 43. The nodes of the model at the bottom line are blocked in both the transversal and vertical direction and those at the top line are blocked in the transversal direction. In addition, the central nodes at both the bottom and top lines are blocked in the lateral direction to restrain rigid body movement while allowing unrestrained thermal expansion. The self-weight is applied on each shell element. After a sensitivity analysis, a mesh size of 4 by 12 elements show convergence of the solution and is therefore adopted for the parametric analyses.

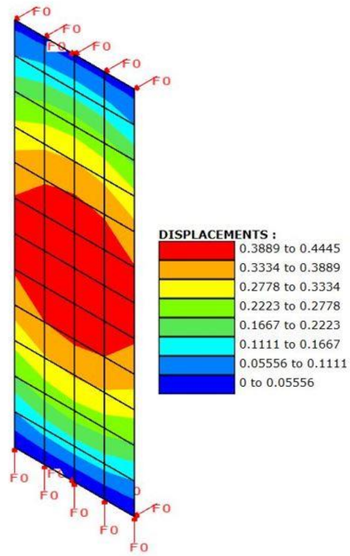

Figure 43. Structural finite element model with transversal (out-of-plane) displacements at 90 min.

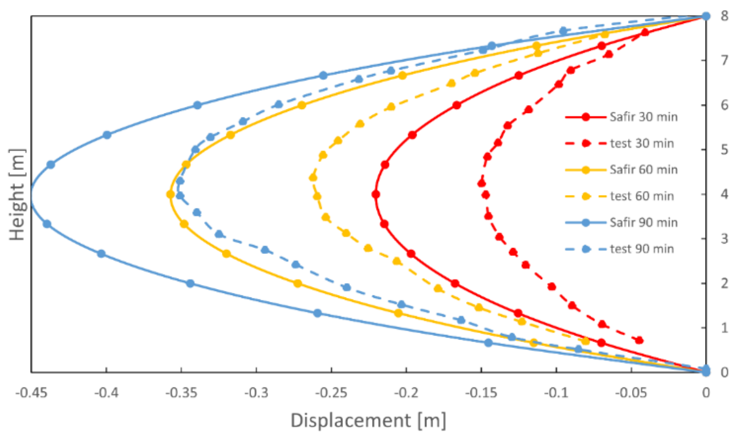

(a) Elevation

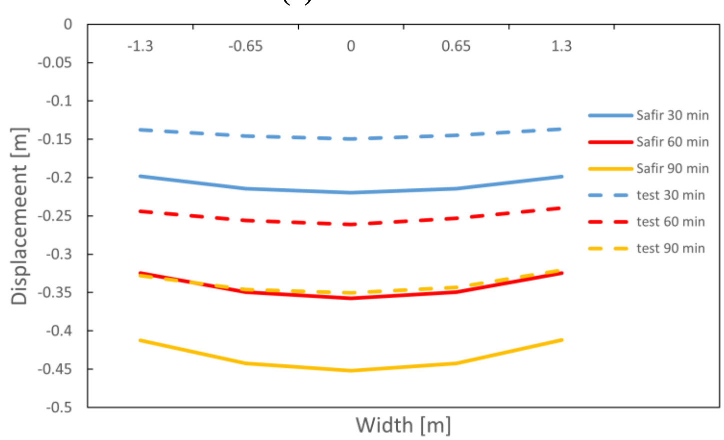

(b) Top view, mid-height

Figure 44. Deflection shape of the wall.

Figure 44 shows the comparison of the deflection results from the structural analysis with the test results. The wall exhibit a two-way curvature due to the thermal and mechanical boundary conditions. The maximum deflections develop in the central zone. The model capture the global behavior, but the values of the out-of-plane displacements predicted by the model overestimate those of the test.

Next, the numerical model was used to evaluate the load capacity of the wall at ambient temperature. A uniformly distributed line loading was applied at the top of the wall and progressively increased until failure. Figure 45 plots the evolution of the transversal displacement at mid-height. The wall collapsed for an applied vertical load of 2412 kN.

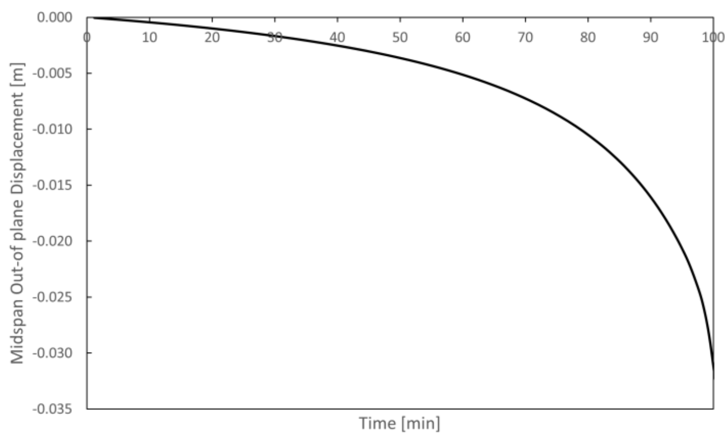

Figure 45. Evolution of midspan out-of-plane displacement of the wall under loading at ambient temperature (loading is increased proportionally with time).

4.4.3 Numerical results

The numerical model benchmarked against the test in the previous section is used to evaluate the fire resistance and DHP of the RC wall under different load ratios. The load ratio is defined as the ratio between the load applied on the wall and the load capacity at ambient temperature evaluated numerically. The DHP is evaluated using the approach of Section 5.1. Only one cooling rate is used, corresponding with the parametric fire model (Eq. 3-2).

The computed DHP are given in Table 11. The DHP (or burnout resistance) is the shortest duration of the heating phase of the applied natural fire model leading to failure of the wall. Figure 46 plots the relationship between R and DHP for the studied walls. As for the RC columns and beams, an approximately linear relationship is observed.

From Table 11, it is observed that the high-rise wall is very sensitive to loading under one-sided fire exposure. The 8-meter wall loaded at 10% of its ultimate load capacity has a standard fire resistance of 26 min. This is due to the large second-order effects exacerbated by the thermally-induced curvature for such slender wall. At a given load ratio, the 4.2-m wall has significantly larger values of R and DHP than the 8-m wall. This indicates that a wall with high slenderness has a higher susceptibility to one-sided fire exposure than a shorter, more compact wall.

Table 11. Results of the fire resistance and DHP numerical analyses for two RC walls under various loads.

Height (m) \ Load ratio		0.01	0.02	0.03	0.04	0.05	0.06	0.07	0.08	0.09	0.1
4.2	R (min)	223	171	141	117	105	92	76	70	63	56
	DHP(min)	206	150	120	104	86	68	61	52	47	41
8	R(min)	133	108	88	67	54	45	38	32	29	26
	DHP(min)	111	91	71	51	37	27	22	17	12	10

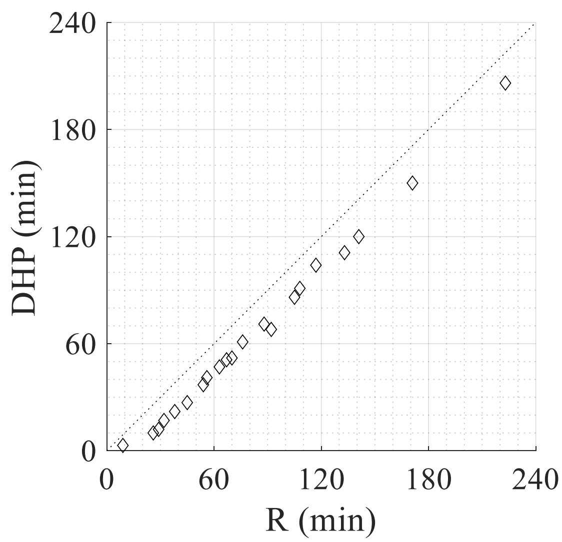

Figure 46. DHP-R relationship for the RC wall.

4.5 Prestressed concrete slabs

4.5.1 Prototypes

The fire resistance tests on prestressed concrete slabs by Maluk et al. [15] are used to benchmark the numerical model with SAFIR for prestressed concrete members. The dimension, loading, supports and materials are presented in Table 12. The specimens were exposed to standard ISO834 fire on three sides until failure. The failure mode was by loss of anchorage and longitudinal splitting cracks as shown in Figure 49.

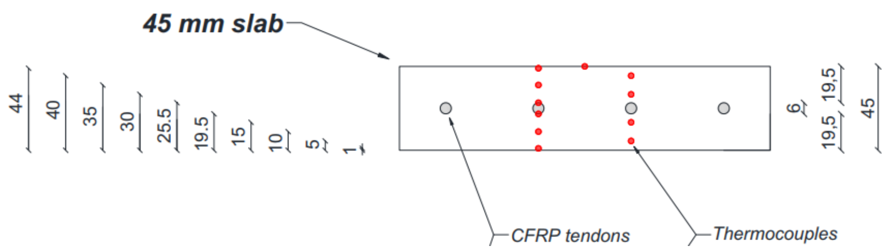

Figure 47. Dimension of cross section of the prestressed concrete slab.

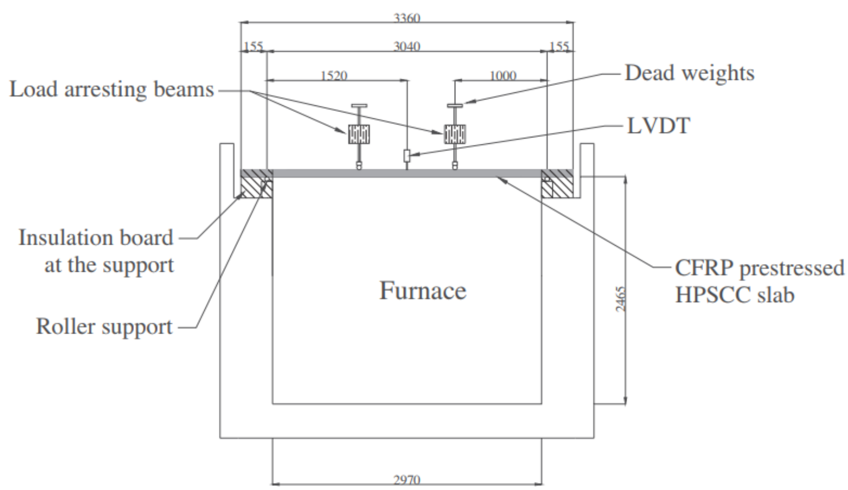

Figure 48. Test setup and loading for the fire resistance tests.

Figure 49. Longitudinal splitting cracks before failure.

Table 12. Test parameters for the prestressed concrete slab.

Applied load (N)	Moisture content	Concrete		Tendon		
		Compressive strength(MPa)	Tensile strength(MPa)	Tensile strength(MPa)	Design elastic modulus(GPa)	Prestress(MPa)
250	3.9%	98.5	5.57	2000	150	1000

4.5.2 Numerical model

The thermal and structural analysis of the prestressed concrete slabs are conducted with SAFIR. The inputs of Table 12 are used in the model.

For thermal analysis, 2D solid elements are used. The discretization of the cross section is shown in Figure 50. The numerical model captures the evolution of the temperatures across the thickness of the slab, as shown in Figure 51 for the mid-span section. The temperature of the tendons measured at mid-span are compared with the numerical results in Figure 52.

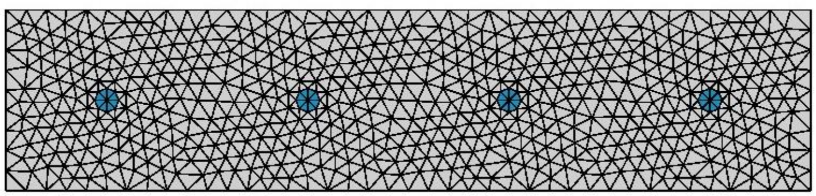

Figure 50. Discretization of cross section in SAFIR for the thermal analysis.

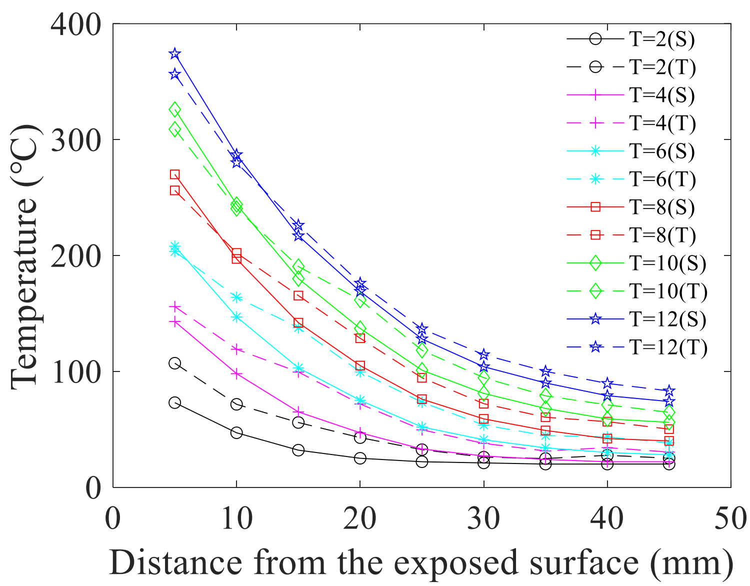

Figure 51. Comparison between computed and measured temperatures in prestressed concrete slabs: (T):test; (S): SAFIR; T=2(S) means the temperature calculated by SAFIR at 2 minutes.

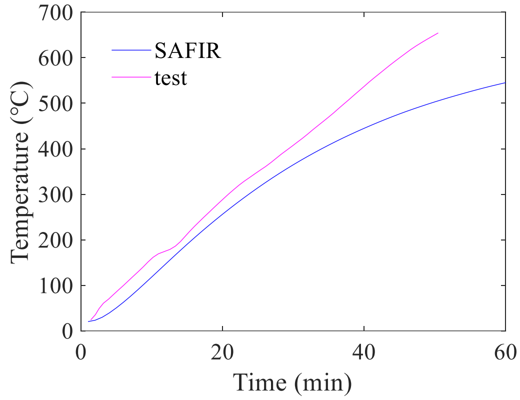

Figure 52. Temperatures of tendons measured during the test and calculated by SAFIR.

For the structural analysis, beam finite elements are used. The material models 'PSTEELA16' and 'SILCON_ETC' are used for tendons and concrete, respectively. The prestressed concrete slabs are stressed prior to the application of external load, through definition of an initial stress in the tensioned tendons. In the numerical model with beam-type finite element, failure by bond degradation between the tendons and the concrete is not captured. Meanwhile, the model is very ductile because the distance between the tendons and the upper fiber is only 22.5 mm, resulting in a large curvature before either material reaches its limit strain. Therefore, the failure mode that is considered in the simulation is by excessive deformation of the prestressed beam. A displacement failure criteria applicable to standard testing is applied, according to the criteria in the ISO standard (as described in [16]). This leads to $D = L^2/400d = 520\ mm$ as the maximum allowable displacement for the beam. Failure is deemed to occur when the displacement exceeds this value at any of the nodes in the model (it occurs at mid-span). Comparison of mid-span vertical displacement measured during the test and calculated by SAFIR is shown in Figure 53. In the test, the early stage was governed by the thermal bowing, followed by an increase of midspan deflection slope due to loss of anchorage. Some discrepancy in the displacement evolution is observed between the test and SAFIR, which may be caused by differences in the temperature distributions and by the effects of bond strength loss. Nevertheless, the displacement at the time of failure (46 min in the test) is reasonably captured.

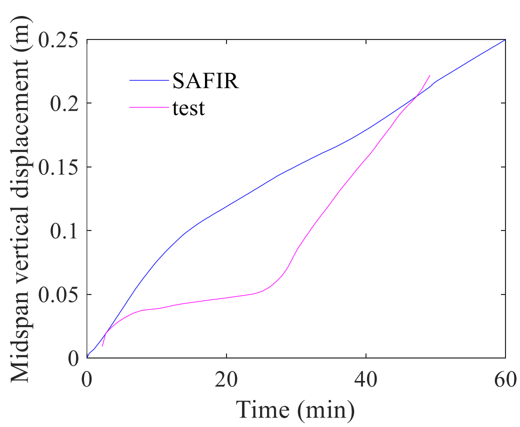

Figure 53. Vertical displacement at mid-span measured during the test and calculated by SAFIR.

4.5.3 Numerical results

The numerical model benchmarked against the test is then used to evaluate the fire resistance and DHP of the prestressed slabs. Load ratios ranging from 0.1 to 0.6 of the ambient temperature capacity are used. The maximum load based on ambient temperature capacity is 3664 kN.

For the DHP evaluation, cooling rates *K* of the standard natural fires ranging from 2 °C/min to 20 °C/min are considered. The result are given in Table 13. The load ratio and cooling rate affect the DHP.

Figure 54 plots the relationship between the standard fire resistance and the DHP obtained with the cooling rate from Eq. 3-2. Figure 55 shows the effect of the cooling rate on the DHP of the prestressed concrete slabs. The six curves represent the 6 loading levels in Table 13. The results show the same trend as for columns and beams in Sections 5.2 and 5.3. The DHP increases with *K*, indicating the slab is more likely to fail during cooling when the cooling rate *K* is lower.

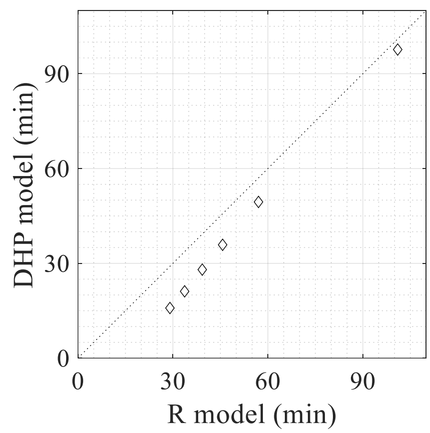

Figure 54. Relationship between R and DHP for the slabs (considering the standard natural fire with a cooling rate following the parametric Eurocode fire).

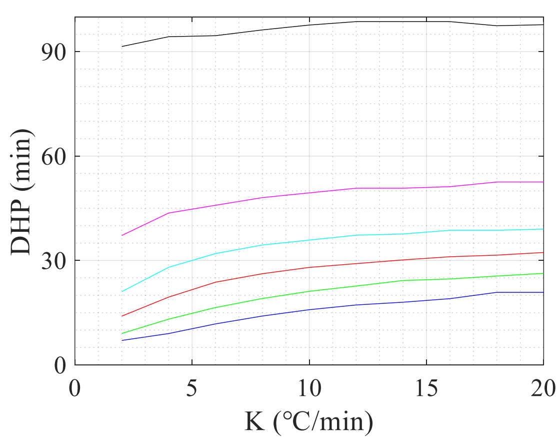

Figure 55. Results of the DHP evaluation for the slabs, as a function of the cooling rate.

Table 13. Fire resistance and burnout resistance (DHP) of prestressed concrete slabs.

Case	Point load (N)	Load ratio	R (min)	K (°C/min)	DHP (min)
1	366	0.1	102	2	91
				4	94
				6	95
				8	96
				10	98
				12	99
				14	99
				16	99
				18	97
				20	98
2	733	0.2	57	2	37
				4	44
				6	46
				8	48
				10	49
				12	51
				14	51
				16	51
				18	53
				20	53
3	1099	0.3	46	2	21
				4	28
				6	32
				8	34
				10	36
				12	37
				14	38
				16	39
				18	39
				20	39
4	1466	0.4	39	2	14
				4	19
				6	24
				8	26
				10	28
				12	29
				14	30
				16	31
				18	32
				20	32
5	1832	0.5	34	2	9
				4	13
				6	16
				8	19
				10	21
				12	23
				14	24
				16	25
				18	26
				20	26
6	2199	0.6	29	2	7
				4	9

6	12
8	14
10	16
12	17
14	18
16	19
18	21
20	21

4.5.4 Simplified approach

The simplified approach described and applied in Section 4.3.4 is used. Since the slabs are prestressed, the following additional assumptions have to be introduced:

- prestressing level does not affect the failure of the member: this assumption is consistent with the ductility of the prestressing steel, and also by the fact that the prestressing steel, subjected to tension, is more affected by fire than the compressed concrete;
- the decay of the prestressing steel follows the curve provided in EN 1992-1-2 for Class B prestressing steel (cold worked).

The results of the calculations are shown in Figure 56. Differently form the case of the prototype beams, here there is an almost perfect agreement between the maximum decay evaluated numerically and the load ratio. This is probably due to the fact that in this case there is only one layer of reinforcement and the heat transfer is one-dimensional, while in the prototype beams there was a variability in the thermal field related to the presence of corner and axis rebars and to the two-dimensional heat transfer.

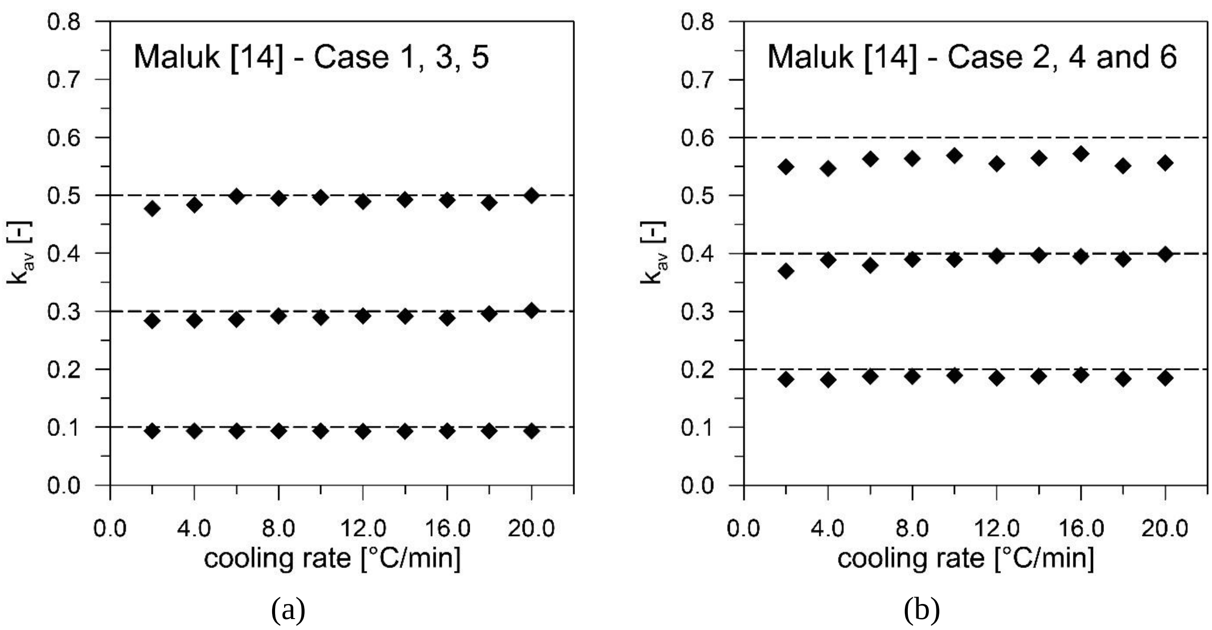

Figure 56. Results of the simplified approach based on minimum strength retained in the lower reinforcement applied to the prototype slabs: (a) Case 1, 3 and 5. (b) Case 2, 4 and 6.

5. Design methods

This task investigates the development of design methods for achieving resistance to full burnout. These design methods can rely on numerical datasets generated from validated finite element models, as presented in the previous section. It is also useful to adopt a template for design provisions that aligns with current practice for standard fire resistance rating. Notably, tabulated data in ACI [17] and other codes can be amended to directly provide the concrete cover and section size to reach specified burnout resistance.

5.1 Application of the burnout resistance to tabulated data

Tabulated data are the most popular and widely used method for designing concrete members in fire conditions. They are featured both in ACI-216 and Eurocode EN 1992-1-2. Typical provisions concern the minimum dimensions of the structural members as well as the axis distance of the main reinforcement from the exposed surface(s). The aforementioned values are determined under the assumption of standard fire exposure, by limiting the rise in temperature to predefined values. These values are determined in such a way as to ensure that the decay of the mechanical properties of concrete and reinforcing steel do not exceed critical values, which are a function of the strength decay curves as well as of the load ratio of the structural member.

5.1.1 ACI provisions for concrete floors – minimum thickness

In this section, ACI provisions for concrete floors are evaluated in light of the heating and cooling phases of natural fires. The objective is to re-evaluate tabulated data for satisfying criteria during the whole duration of natural fires. For concrete floors, minimum thickness requirements must be met for purposes of barrier fire resistance (Table 14).

Table 14. Fire resistance of single-layer concrete walls, floors, and roofs (from ACI 216).

Aggregate type	Minimum equivalent thickness for fire-resistance rating, mm				
	1 hour	1-1/2 hours	2 hours	3 hours	4 hours
Siliceous	90	110	125	155	175
Carbonate	80	100	115	145	170
Semi-light-weight	70	85	95	115	135
Lightweight	65	80	90	110	130

The analyses consider solid slabs with flat surfaces made of concrete with siliceous aggregates. Design of the thickness is taken according to the tabulated data. Thermal analyses of the slabs are run to check the minimum thickness criteria. The thermal analyses use 2D model of the cross-section as shown in Figure 57 and validated in Section 4. For the thermal boundary conditions, the lower face of the slab is subjected to the relevant fire curve, i.e., either ASTM E119 (for fire resistance) or the standard natural fires used for evaluating DHP. The upper face is in contact with air at ambient temperature, while the sides have adiabatic frontiers to represent continuity in the plane of the floor. The material properties are taken from Eurocode for a siliceous concrete.

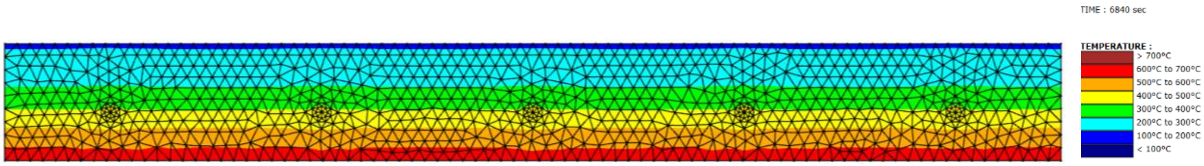

Figure 57. Cross-section discretization and temperature distribution for the slab with thickness of 110 mm and cover of 40 mm under a fire with DHP of 79 min.

The thermal analyses allow checking the barrier fire resistance criteria. Criteria provided in ASTM E119 are designed for standard fire exposure and therefore apply to the heating phase of the fire, until time of peak gas temperature. For thickness, the relevant criterion is as follows:

- The average temperature rise on the unexposed surface shall be smaller than 250 °F (139 °C). (Note: this is a temperature rise, so assuming an initial temperature of 20 °C, the temperature should not exceed 159 °C).

In addition, the Eurocode EN1992-1-2 provides a thermal barrier fire resistance criterion applicable to the cooling down phase. This criterion is adopted herein:

- During the cooling phase, the average temperature rise on the unexposed surface shall be smaller than 392 °F (200 °C). (Note: this is a temperature rise, so assuming an initial temperature of 20 °C, the temperature should not exceed 220 °C).

The results are shown in Table 15. Slabs with thickness taken from the ACI tabulated data are analyzed. First, it is confirmed that the fire resistance specified in the ACI table is reached: the time at which the barrier fire resistance criteria is met in the numerical simulation is larger than the rating in the ACI table. Then, the maximum DHP is found for which the barrier fire resistance criteria are satisfied with the specified design. For example, for the 90 mm thick slab, the average temperature rise on the unexposed surface remains smaller than 392 °F as long as the duration of heating phase of the natural fire remains smaller or equal to 43 minutes. For a heating phase longer than 43 minutes, the unexposed surface will reach a temperature higher than 392 °F at some point during the cooling phase due to the continued heat transfer, such that the barrier criteria are not satisfied (see Figure 58). Table 15 shows that the DHP is shorter than R for thickness of 125 mm or less, while for thickness larger than 125 mm, the criterion in the cooling phase is not governing and DHP and R are equal.

Thermal analyses can also be used to determine the minimum thickness for burnout-resistance rating. Iterative analyses are conducted by subjecting slabs of varying thickness to specified duration of natural fire, for the whole heating and cooling phase, until finding the thickness that satisfies the barrier criteria. For example, to limit the temperature rise on the unexposed face to 392 °F during the cooling phase of a 1-hour natural fire, the minimum slab thickness is 105 mm. Results are reported in Table 16. The thickness for burnout-resistance rating is larger than that for fire-resistance rating because of the continued heating of the section and temperature rise on the unexposed face during the cooling phase.

Table 15. Fire-resistance and burnout-resistance ratings (fire barrier criteria) as a function of the equivalent thickness, mm. Slab with siliceous aggregates concrete.

R rating	**1 hour**	**1-1/2 hours**	**2 hours**	**3 hours**	**4 hours**
thickness (mm)	90	110	125	155	175
R (min)	64	93	120	185	240
DHP (min)	43	76	108	183	240

Table 16. Minimum equivalent thickness for burnout-resistance rating (fire barrier criteria), mm. Siliceous aggregates concrete.

DHP rating	**1 hour**	**1-1/2 hours**	**2 hours**	**3 hours**	**4 hours**
thickness (mm)	105	120	130	155	175
R (min)	86	111	130	185	239

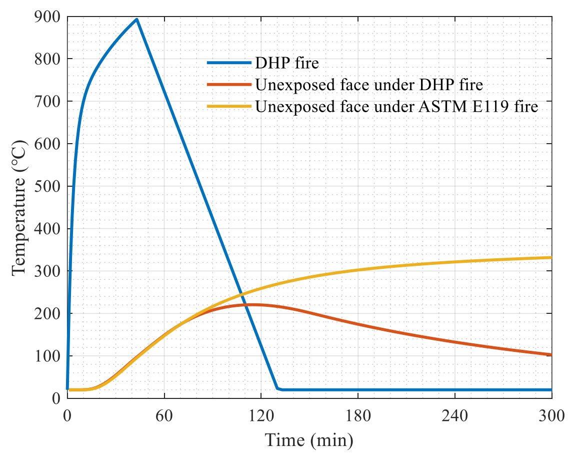

Figure 58. Temperature evolution at the unexposed face of the 90 mm thickness slab for the standard ASTM E119 fire and a fire with DHP of 43 min.

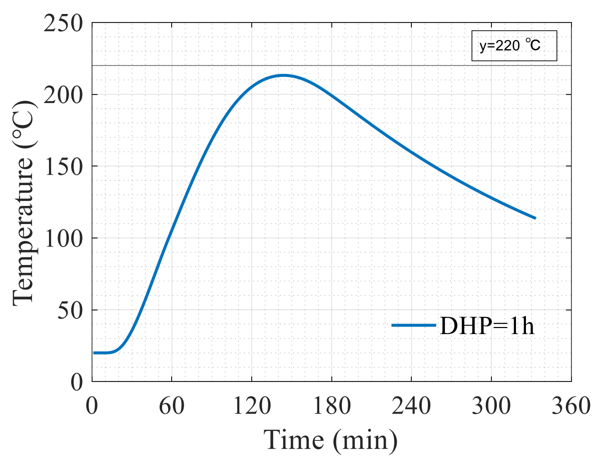

Figure 59. Temperature evolution on the unexposed face of the siliceous concrete slab with thickness of 105 mm when exposed to a fire with DHP 1 hour.

5.1.2 ACI provisions for concrete floors – minimum cover

Cover protection requirements are specified in ACI 216 for the steel reinforcement based on the structural end-point. The minimum thickness of concrete cover over positive moment reinforcement (bottom steel) is given in Table 4.3.1.1 of the ACI code (Table 17). This table is applicable to one- or two-way cast-in-place beam/slab systems or precast solid or hollow-core slabs with flat undersurfaces. Cover is defined from the exposed concrete surface to the surface of the steel reinforcement. These provisions for minimum concrete cover of reinforcement in concrete floors are evaluated in light of the heating and cooling phases of natural fires.

Table 17. Minimum cover in concrete floors and roof slabs (from ACI 216).

Aggregate type	Cover*† for corresponding fire resistance, mm					
	Restrained	Unrestrained				
	4 or less	1 hour	1-1/2 hours	2 hours	3 hours	4 hours
Nonprestressed						
Siliceous	20	20	20	25	30	40
Carbonate	20	20	20	20	30	30
Semi-lightweight	20	20	20	20	30	30
Lightweight	20	20	20	20	30	30
Prestressed						
Siliceous	20	30	40	45	60	70
Carbonate	20	25	35	40	55	55
Semi-lightweight	20	25	35	40	50	55
Lightweight	20	25	35	40	50	55

*Shall also meet minimum cover requirements of 4.3.1.

†Measured from concrete surface to nearest surface of longitudinal reinforcement.

The structural response of the slab at elevated temperature is evaluated using thermal-structural finite element analyses. The analyses are used to determine cover requirements for burnout resistance rating. The analyses consider prestressed concrete slabs with siliceous aggregates. Figure 60 shows the general typology of the one-way prestressed solid slab with flat undersurface, designed for 1 hour fire resistance. The slabs are assumed to be unrestrained. The thickness is 90 mm and the cover is 30 mm according to the tabulated data. Five 7/16 inch tendons (11.1 mm diameter, 96.8 mm^2) are used per meter width. The tendons are grade 270 (1860 MPa) and an 80% prestressing stress is assumed, i.e., the initial stress in the tendons is 215 ksi (1488 MPa). The concrete compressive strength is 6 ksi (41 MPa). The prestressed slab is assumed to be simply supported with a span of 3 m. The loading is determined as 0.35 times the ultimate load at ambient temperature evaluated using the numerical model.

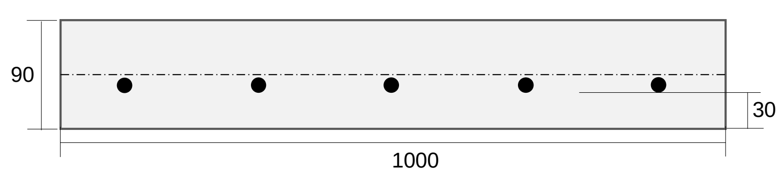

Figure 60. Prestressed slab design for 1 hour fire resistance according to tabulated data.

First, analyses are conducted under standard ASTM E119 fire. The fire resistance time is evaluated as the time of failure (loss of stability) of the slab under the applied loading and standard fire exposure. The obtained fire resistance is given in Table 18. It exceeds the fire resistance rating, confirming the designs of the tabulated data.

Then, analyses are run under standardized natural fires to obtain the DHP for each tabulated design. Cooling rates from 2 to 20 ℃/min are considered. Results are given in Table 18 and plotted in Figure 61.

Table 18. Fire-resistance and burnout-resistance ratings (loadbearing capacity criteria) as a function of the cover, mm. Siliceous aggregates concrete.

R rating		**1 hour**	**1-1/2 hours**	**2 hours**	**3 hours**	**4 hours**
cover (mm)		30	40	45	60	70
thickness (mm)		90	110	125	155	175
applied load (kN/m)		11.22	13.73	17.00	21.41	26.60
applied load ratio		0.35	0.35	0.35	0.35	0.35
R (min)		84	127	151	208	263
DHP (min)	K=2 (°C/min)	38	59	73	90	138
	K=4 (°C/min)	55	81	99	126	176
	K=6 (°C/min)	62	92	110	142	189
	K=8 (°C/min)	67	96	116	151	196
	K=10 (°C/min)	69	100	118	156	201
	K=12 (°C/min)	69	102	121	160	205
	K=14 (°C/min)	70	104	123	164	208
	K=16 (°C/min)	70	104	124	165	209
	K=18 (°C/min)	73	106	125	166	212
	K=20 (°C/min)	73	106	125	168	212

Finally, new tabulated data can be derived to achieve specified burnout-resistance ratings. These tabulated data are obtained with the standardized natural fire (i.e., K = 10.4 ℃/min) and with the applied load specified in Table 18. Table 18 provides the minimum cover for slabs with thickness according to the current tabulated data (derived for fire-resistance thermal barrier). The thickness satisfies the thermal barrier criterion during the heating phase (fire resistance) but not during the cooling phase. Table 19 provides the minimum cover for slabs with thickness that satisfies the heat-transmission end point up to full burnout, as derived in Table 16.

Temperature distributions in the slab are shown in Figure 62. These distributions are plotted at the time of failure for the slab designs that are in accordance with the fire resistance tabulated data but fail during the cooling phase when subjected to the standardized natural fire of the same heating duration as the fire rating followed by a cooling phase. The temperature in the tendons ranges between 400 ℃ and 500 ℃ at the time of failure.

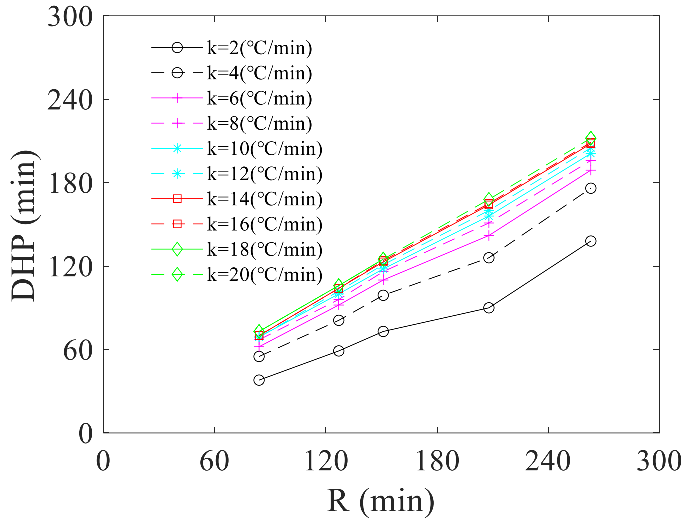

Figure 61. Fire resistance R and burnout resistance DHP of the prestressed concrete slabs (DHP is given for fires with different cooling rates K).

Table 18. Minimum cover for burnout-resistance rating in prestressed concrete slabs, mm. Siliceous aggregates concrete. Thickness satisfies heat-transmission end point for fire resistance.

DHP Rating	**1 hour**	**1-1/2 hours**	**2 hours**	**3 hours**	**4 hours**
Thickness (mm)	90	110	125	155	175
Cover for R (mm)	30	40	45	60	70
Cover for DHP (mm)	30	40	50	NP	NP

Table 19. Minimum cover for burnout-resistance rating in prestressed concrete slabs, mm. Siliceous aggregates concrete. Thickness satisfies heat-transmission end point for burnout resistance (i.e., criteria applicable for cooling).

DHP Rating	**1 hour**	**1-1/2 hours**	**2 hours**	**3 hours**	**4 hours**
Thickness (mm)	105	120	130	155	175
Cover for R (mm)	30	40	45	60	70
Cover for DHP (mm)	30	40	50	NP	NP

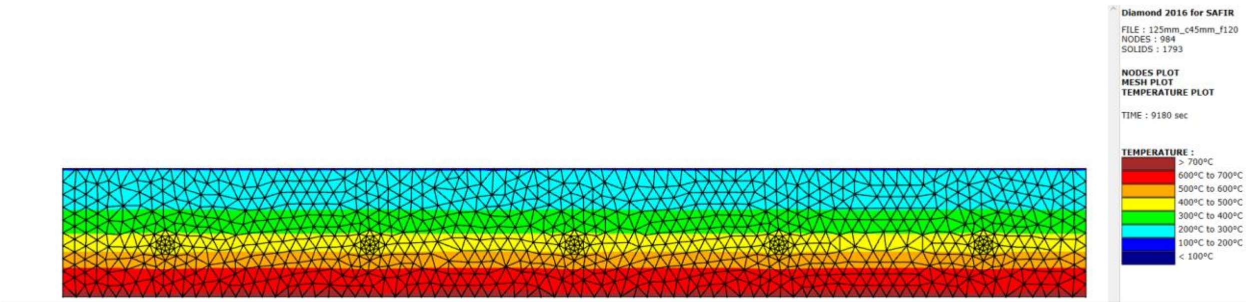

DHP=2 h, thickness=125mm, cover=45mm

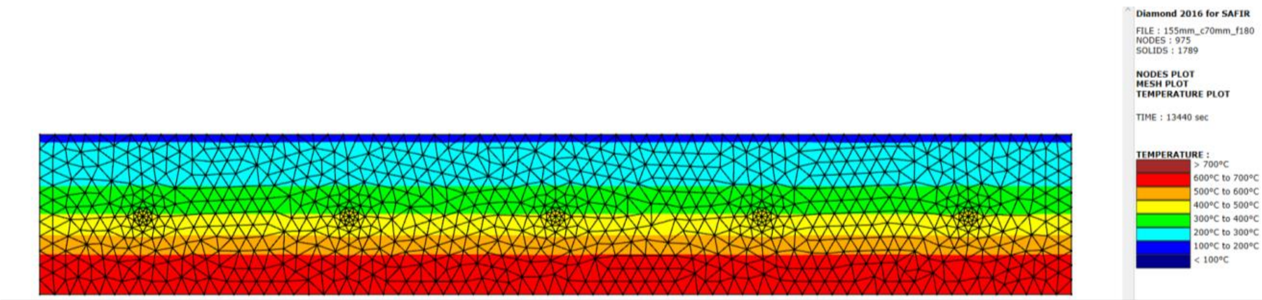

DHP=3h, thickness=155mm, cover=70mm

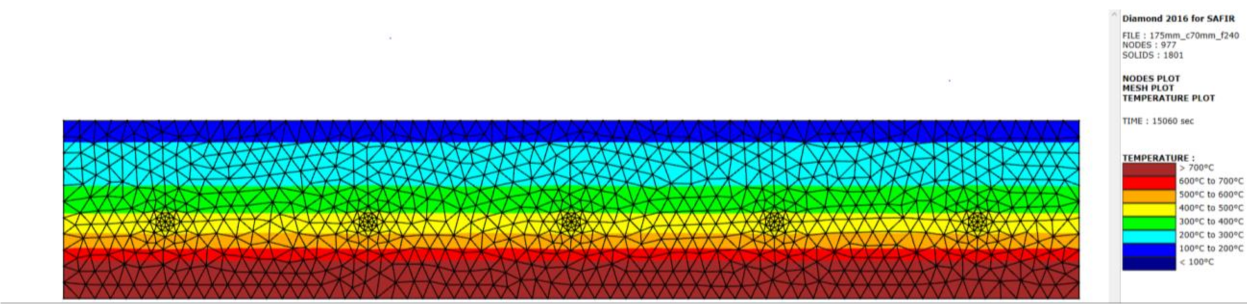

DHP=4h, thickness=175mm, cover=70mm

Figure 62. Temperature distributions in the prestressed concrete slabs at the time of failure during the cooling phase of the standardized natural fires.

5.1.3 Simplified approach

The simplified approach described and applied in Section 4.3.4 is used. As in the previous section concerning the prototype prestressed slabs, prestressing level is assumed not to affect failure, and prestressing steel decay is assumed to follow the curve provided in EN 1992-1-2 for Class B prestressing steel (cold worked).

For the fire resistance classes from 1 hour to 2 hours, there is once again a very good agreement between the maximum calculated retaining factor and the load factor. On the contrary, for the dimensions corresponding to a fire resistance class of 3 hours, there appears to be an overestimation of the bearing capacity during the design fire scenarios, since the maximum retaining factor is larger than the load factor (thereby indicating that, according to the simplified approach, no failure would take place for the considered fire scenarios). This result is due to the differences in the modelling assumptions concerning the thermal field: notably, in the thermal models used for the advanced analyses, the rebars are included in the FE mesh of the section: looking at the results shown in Figure 62, the effect of the steel tendons on the temperature distribution are visible, with higher temperatures attained in comparison to the adjacent points. The simplified analyses were carried out without considering the presence of the tendons, as it is usually done in design and assessment; therefore, slightly lower temperatures are attained at the level of the tendons: as a matter of fact, the maximum temperature resulting from the calculations is equal to ≈ 415°C, while the temperature required for the attainment of a retaining factor equal to the load ratio (= 0.35) is 446°C.

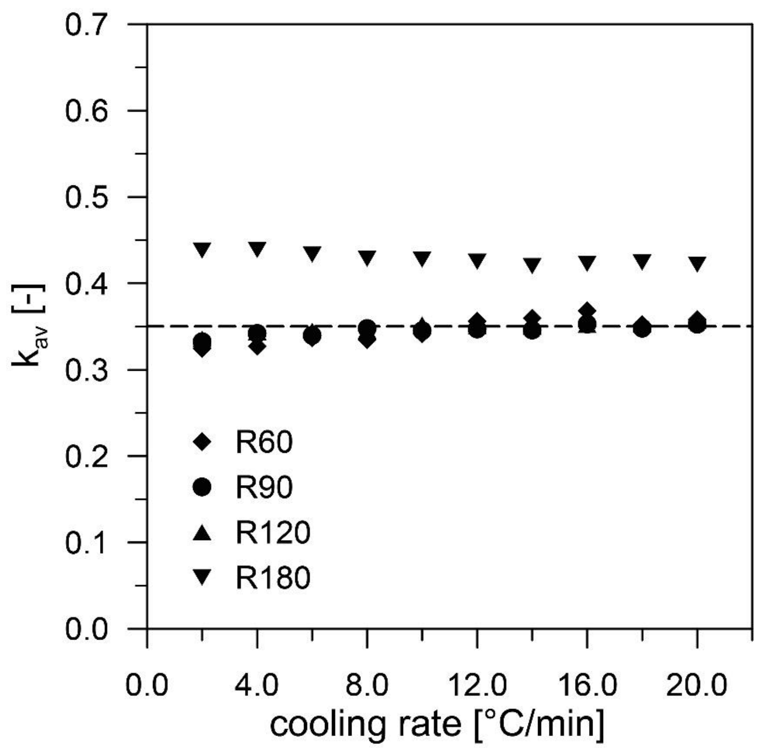

Figure 63. Results of the simplified approach based on minimum strength retained in the lower reinforcement applied to the ACI provisions for slabs.

5.1.4 ACI provisions for concrete beams – minimum cover

For concrete beams, the minimum thickness of concrete cover over non-prestressed flexural reinforcement is given in Table 4.3.1.2 of the ACI code (Table 19). ACI 216 states that "The concrete cover for an individual reinforcing bar is the minimum thickness of concrete between the surface of the reinforcing bar and the fire-exposed surface of the beam. For beams in which several reinforcing bars are used, the cover, for the purposes of Table 4.3.1.2, is the average of the minimum cover of the individual reinforcing bars. For corner reinforcing bars (that is, reinforcing bars equidistant from the bottom and side), the minimum cover used in the calculation shall be half the actual value." These provisions for minimum concrete cover of reinforcement in unrestrained concrete beams are evaluated in light of the heating and cooling phases of natural fires to evaluate ability to resist through burnout.

Table 19. Minimum cover in non-prestressed beams (from ACI 216).

Restraint	Beam width, mm	Cover for corresponding fire-resistance rating, mm				
		1 hour	1-1/2 hours	2 hours	3 hours	4 hours
Restrained	125	20	20	20	25	30
	175	20	20	20	20	20
	≥250	20	20	20	20	20
Unrestrained	125	20	25	30	NP	NP
	175	20	20	20	45	75
	≥250	20	20	20	25	45

Note: NP = not permitted.

Reinforced concrete beams are designed based on the tabulated data. The considered section dimensions are (b x h) 125 x 300 mm^2, 175 x 400 mm^2 and 250 x 600 mm^2. The spans are 2.5 m, 3.0 m, and 5.0 m, respectively, and the beams are simply supported. Siliceous aggregates concrete is adopted. The number and dimensions of reinforcing bars is selected to satisfy the minimum ratio of reinforcement and the maximum ratio for ductile tensile limit state. The beams are reinforced with single rebar or corner rebars. The load ratio is back-calculated to achieve the required fire resistance ratings from Table 19 with the designed beams when numerically evaluating their fire resistance. Inputs are given in Table 20.

Table 20. Dimensions and inputs of the studied reinforced concrete beams.

b (mm)	h (mm)	cover (mm)	d (mm)	length (m)	rebar no.	no. of rebars	load (N/m)	load ratio	R FEM (min)	R ACI 216 (min)
125	300	25	269	2.5	8	1	19,400	0.32	97	90
125	300	30	264	2.5	8	1	15,800	0.30	126	120
175	400	20*	354	3	8	2	49,560	0.45	122	120
175	400	45	346	3	11	1	31,930	0.30	184	180
250	600	20*	552	5	10	2	69,420	0.65	120	120
250	600	25*	542	5	10	2	44,960	0.43	187	180
250	600	45*	502	5	10	2	62,010	0.65	248	240

*the actual cover in the model is double this value because two corner reinforcing bars are used.

The beams are modeled in the finite element software SAFIR. The 2D thermal analysis of the beam section uses the same method as validated in Section 4.3. For the thermal boundary conditions, the lower face and two lateral sides of the beam are subjected to the relevant fire curve, i.e., either ASTM E119 (for fire resistance) or the standard natural fires used for evaluating DHP, while the upper face is in contact with air at ambient temperature. The material properties are taken from Eurocode for a siliceous concrete and assumed irreversible during cooling. The structural analysis is then run to evaluate the structural response under fire. The analyses are used to determine cover requirements for burnout resistance rating. The beams are unrestrained. The reinforcing steel has a yield strength of 60,000 psi (410 MPa). The concrete compressive strength is 4,000 psi (27.5 MPa). The evolution of steel and concrete properties with temperature is taken from the Eurocodes. The material properties used in the model are listed in Table 21.

The calculated DHP for the reinforced concrete beams is given in Table 22. The calculations are made with the inputs of Table 20 and Table 21. The calculated DHP is shorter than the fire resistance rating. Figure 64 and Figure 65 show the temperature distribution in the beam cross sections at the time of failure.

Finally, new tabulated data can be derived to achieve specified burnout-resistance ratings. These tabulated data are obtained with the standardized natural fire (i.e., K = 10.4 ℃/min) and with the beam designs and loading specified in Table 20. Table 23 provides the minimum cover for the non-prestressed beams, which are unrestrained, as a function of their width and rating. The minimum cover for achieving a burnout-resistance rating is typically larger than for the same fire-resistance rating, due to the delayed impact of the fire during the cooling phase.

Table 21. Summary of material properties for the beam.

	Material Properties	Value
Concrete	Specific Mass [kg/m^3]	2400
	Moisture Content [kg/m^3]	48
	Convection Coeff. Hot [W/m^{2}K]	25
	Convection Coeff. Cold [W/m^{2}K]	4
	Relative Emissivity	0.7
	Parameter of Thermal Conductivity	0.5
	Poisson Ratio	0.2
	Compressive Strength [MPa]	27.5
	Tension Strength [MPa]	2.75
Steel	Convection Coeff. Hot [W/m^{2}K]	25
	Convection Coeff. Cold [W/m^{2}K]	4
	Relative Emissivity	0.7
	Young's Modulus [GPa]	210
	Poisson Ratio	0.3
	Yield Strength [MPa]	410

Table 22. DHP for the reinforced concrete beams from Table 20.

b (mm)	h (mm)	cover (mm)	R ACI 216 (min)	DHP (min)
125	300	25	90	71
125	300	30	120	87
175	400	20	120	88
175	400	45	180	133
250	600	20	120	86
250	600	25	180	141
250	600	45	240	158

Table 23. Minimum cover for corresponding fire-resistance and burnout-resistance ratings, non-prestressed unrestrained beams, in mm.

Beam width (mm)	Rating (min)	1 hour	1 ½ hour	2 hours	3 hours	4 hours
125	R	20	25	30	NP	NP
125	DHP	25	35	45		
175	R	20	20	20	45	75
175	DHP	20	25	45		
250	R	20	20	20	25	45
250	DHP	20	25	25		

Note: NP = not permitted.

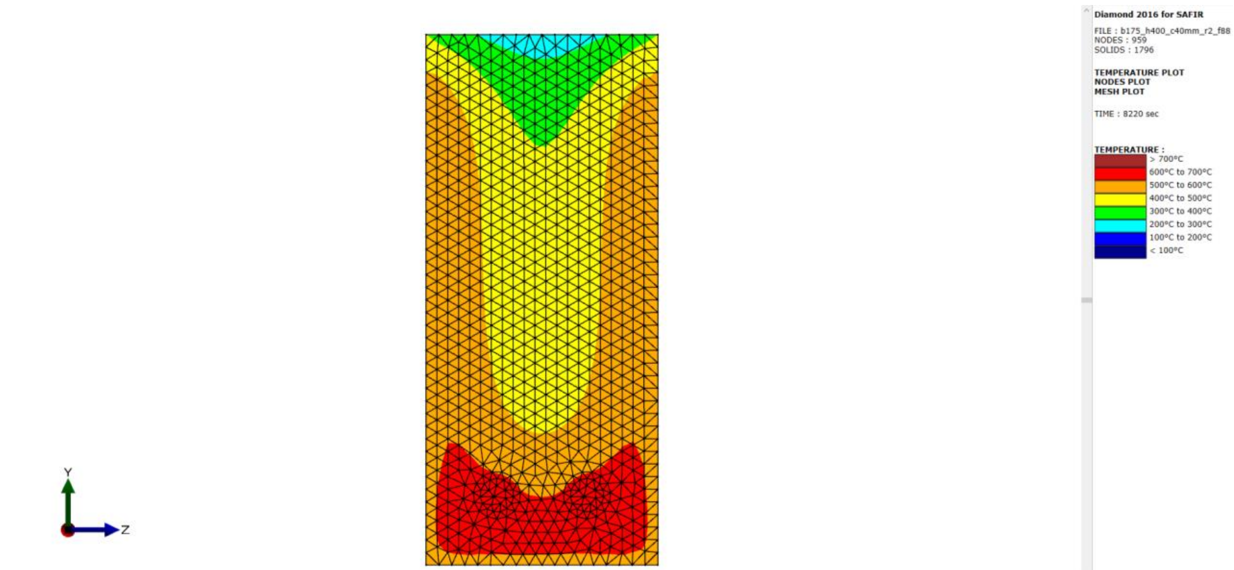

Figure 64. Temperature distribution at the time of failure for the fire with 88 minutes of heating phase, for the the beam with width of 175 mm and cover of 40 mm (note: corresponding to 20 mm for corner rebars in the ACI table).

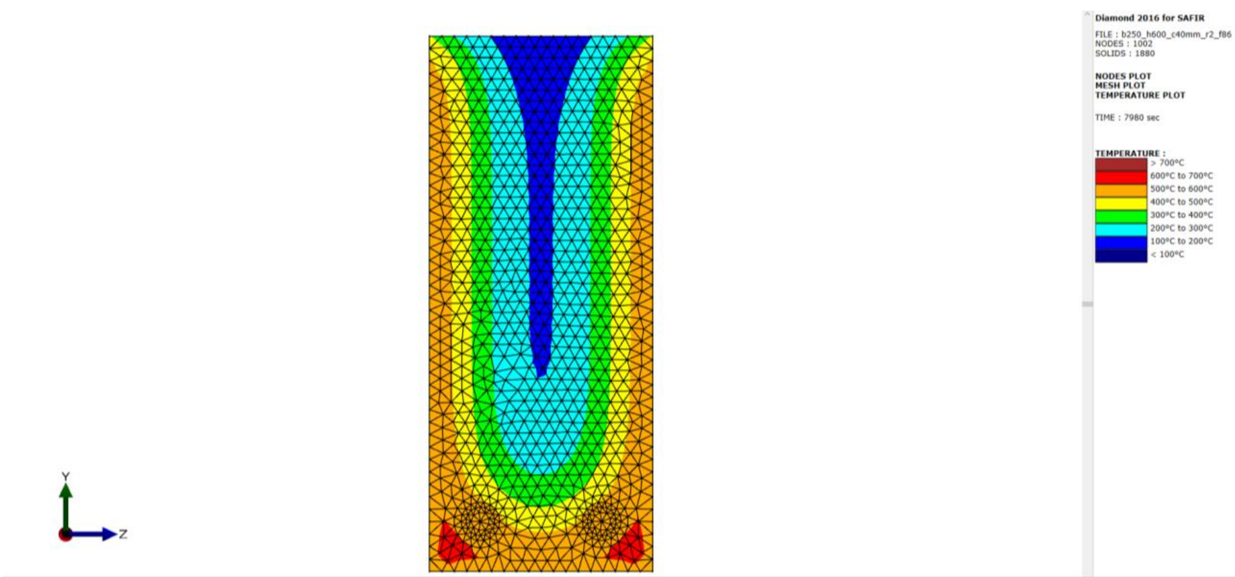

Figure 65. Temperature distribution at the time of failure for the fire with 86 minutes of heating phase, for the beam with width of 250 mm and cover of 40 mm (note: corresponding to 20 mm for corner rebars in the ACI table).

5.2 Regression analysis from the parametric numerical study

In this section, the numerical results of Section 4.2 are used to investigate a design equation format for predicting the DHP for reinforced concrete columns. For the 74 columns, the standard fire resistance R and the DHP computed with different cooling rate K by SAFIR are used to derive the design equation. The cooling rate K varies from 2 °C/min to 20 °C/min as shown in Figure 28.

For the specific case of the cooling from the Eurocode parametric fire model, Eq. 5-1 had been proposed to relate the burnout resistance (DHP) of reinforced concrete columns to their standard fire resistance [8].

$$DHP = 0.72 \times R - 3.0 \qquad \text{(in min)} \qquad \text{(Eq. 5-1)}$$

For generalization, a new regression is derived herein considering the range of cooling rates applied in the parametric numerical simulations of Section 4.2 (Figure 28). The new equation, Eq. 5-2, allows evaluating the burnout resistance (DHP, in min) as a function of the fire resistance (R, in min) and the cooling rate (K, in °C/min).

$$DHP = (0.7 \times R) \times \left(\frac{K}{10}\right)^{0.2} \qquad \text{(in min)} \qquad \text{(Eq. 5-2)}$$

Figure 66 compares the DHP predicted by Equation (5-2) with the DHP calculated by the SAFIR finite element analysis for the 74 columns and 10 cooling rates (Figure 28). The value used for R in the equation is the value evaluated from SAFIR. The plot shows that the proposed equation, while simple, provides a conservative and accurate (R^2=0.95) estimate of the burnout resistance DHP as a direct function of the standard fire resistance R, which captures the effect of different cooling rates.

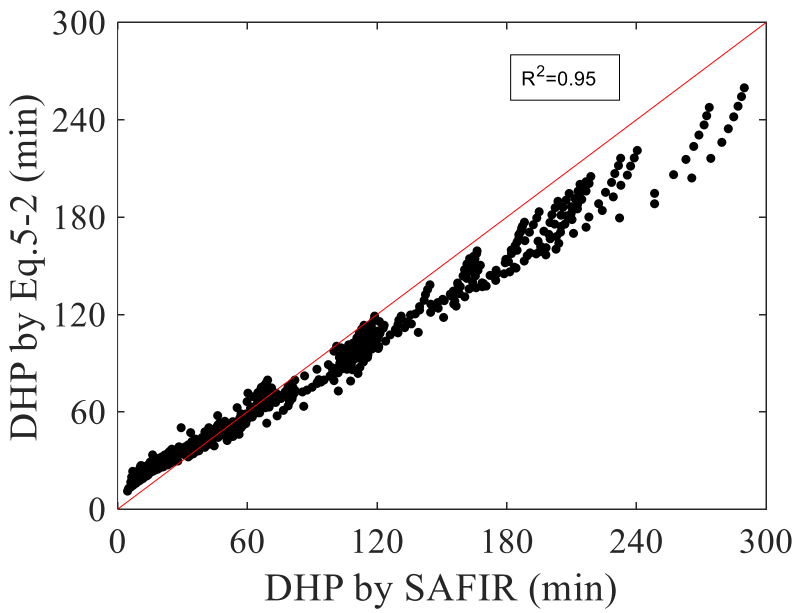

Figure 66. Comparison between DHP evaluated using the simple Eq. 5-2 and DHP computed by FEA with SAFIR.

6. Conclusions and Future Works

This project investigated the behavior and design of reinforced and prestressed concrete structural members under natural fires. The focus was on the improvement of the understanding of the effects of the cooling phases on the loadbearing capacity of concrete members. Based on the work reported in this document, the following key conclusions can be drawn:

Thermal and mechanical properties of concrete during the cooling phase of a fire
Experiments conducted on concrete cylinders made from different mixes showed that the thermal and mechanical properties of concrete are not reversible during cooling.

- The thermal diffusivity, which was found to decrease during heating up to 900°C following a relationship consistent with the current Eurocode EN1992-1-2 provisions, exhibited an approximately constant value throughout cooling. Therefore, it is reasonable to assume that, upon cooling, the diffusivity remains constant, and equal to the value attained at the maximum temperature reached during the thermal cycle.

- Regarding the compressive strength, the experiments showed that the residual strength of concrete is lower than its strength at high temperature, indicating further degradation during the cooling process.

- The data for compressive strength at high temperature generally agreed with the provisions of EN1992-1-2. The data for residual compressive strength (i.e., at 20°C after heating) reasonably agrees with the tentative provisions given in prEN 1992-1-2. When code provisions are adopted, the data support using lower values for the residual strength than for the high temperature strength, as is the case in the tentative provisions in prEN 1992-1-2.

- Further, experiments were made to measure the compressive strength at intermediate temperatures during the cooling process. The data showed that the variation is not linear, in fact exhibiting some strength regain before a further reduction to the residual value. Further research is needed to fully characterize the strength variation throughout the cooling process and, at the material level, elucidate the causes behind these variations.

Proposal of a standardized natural fire exposure
The selection of a standardized natural fire model is deemed necessary to support the development of a simple method for *burnout resistance* design. Physics-based modeling of the fire development in a specific building compartment will always be valuable in a performance-based approach, but to systematically characterize and compare the ability of structural members to survive to burnout, the same natural fire exposure must be consistently applied, just as the ASTM E119 is applied to measure the fire resistance rating. After review of fire models and experimental data on cooling phases, the standardized natural fire model with the following characteristics is proposed:

- Heating following the ISO 834 standard time-temperature curve;

- Cooling linear, at a (constant) cooling rate between 2 °C/min and 20 °C/min.

It is noteworthy that this natural fire model is consistent with the Eurocode EN1991-1-2 parametric fire model, where the parameter Γ is set to unity and the linear cooling rate is adjusted. Using this model, structural members can be tested against various severity of natural fires by adjusting the duration of the heating phase.

Numerical data on the burnout resistance of concrete member

Finite element analysis has been applied to assess the behavior under natural fire of concrete members including reinforced concrete columns, beams and walls, and prestressed concrete slabs. This allowed generating a numerical database of standard *fire resistance* and *burnout resistance* for these members, including the effect of different cooling rates, with the following conclusions:

- The burnout resistance can be quantified through the Duration of Heating Phase (DHP) indicator. The DHP is obtained by varying the duration of the heating phase of the standardized natural fires, until finding the shortest one that the member cannot survive.
- For all studied members, the burnout resistance (DHP) is shorter than the fire resistance (R). This means that concrete members may fail during the cooling phase when exposed to a fire shorter than their fire resistance rating. This results mostly from delayed heat transfer in the sections of the members, while additional reduction of compressive strength and variations in strains/deformations during cooling also play a role.
- Slower cooling rates result in lower DHP. In other words, after being exposed to heating for a certain duration, a concrete member is more likely to survive to burnout if the air temperature in the room goes down back to ambient faster rather than slower.
- Evaluating the burnout resistance of a concrete member requires performing a thermal-mechanical analysis of the member throughout the fire history. The DHP cannot be evaluated solely from a thermal analysis, because different temperature distributions in the section may result in failure during the cooling phase, for instance depending on the cooling rate.
- At a given cooling rate, the burnout resistance is approximately proportional to the fire resistance. The coefficient of proportionality is lower than 1.0 and depends on the typology of the concrete member.

Design methods for burnout resistance

Finally, design methods have been proposed to achieve resistance to full burnout under standardized natural fires. Three approaches have been presented, including tabulated data, a simple equation relating DHP to R, and a simplified method based on the reinforcement temperature. The following conclusions can be drawn:

- It is possible to derive tabulated data, in a format similar to that in the current ACI 216 standard, giving provisions for burnout resistance design.
- Tabulated data were provided for the minimum thickness and cover requirements for concrete floors and beams. These data show that, in most cases, it is possible to upgrade the performance objective from *fire resistance* to *burnout resistance* for a same duration

of heating exposure with relatively minor increases in cover and/or thickness of the concrete members. In other words, the structural upgrades to account for the effects of the cooling phase and the possibility of delayed failure are generally modest. Note that it is not suggested that design requirements should necessarily be increased to achieve resistance to burnout under the same duration of heating as currently considered for the fire resistance rating. Rather, the burnout resistance design method provides an approach to demonstrate stability until full burnout, but the question of what the required objective should be is still to be addressed.

- For reinforced concrete columns, a simple equation allows evaluating the burnout resistance as a function of the fire resistance and the cooling rate.
- A simplified approach, based on the consideration of the temperature reduction of the mechanical properties of the reinforcement in the critical section for statically determinate members, has been shown to be accurate for concrete slabs and conservative for concrete beams. This approach can be a powerful method to quickly evaluate the ability of a concrete member to survive until burnout, but further research is recommended to confirm the range of applicability and improve agreement in the case of the beams.

Future work

Based on the work conducted and the conclusions formulated above, a number of key suggestions for future work are given below.

- Although this work provided very valuable data on the concrete properties during cooling and in the residual state, more experimental research is needed to complement these tests and improve understanding of the material behavior. First, other concrete mixes should be tested under the protocol established in this research. This could include other calcareous aggregate types, as well as high strength concretes, amongst others. Then, further research on the evolution of the strength at intermediate temperature during the cooling process is needed, based on the observation that the strength exhibited a regain followed by a more dramatic reduction. To investigate this issue, cylinder tests should be complemented with investigation of the physico-chemical phenomena in the material. It would also be interesting to explore the effect of different cooling rates on the residual mechanical properties of concrete. Indeed, it has been observed through finite element simulations that faster cooling rates were more favorable for maintaining stability indefinitely, however, these simulations assumed that the material behavior was independent of the cooling rate, which may not be the case.
- This work has presented a methodology to derive simple design methods for burnout resistance, based on advanced numerical modeling of the thermal-mechanical response of concrete members. A procedure to derive tabulated data and simple equations has been developed and applied to selected concrete structural members. Other typologies of concrete elements could be studied following the same approach, to build tabulated data and simple equations for burnout resistance design.

- The simplified approach adopted in this work, adopted from EN 1992-1-2 (Annex E) and extended to the case of natural fires, proved overly conservative for some cases. Future work could focus on refining this approach and improving accuracy for natural fires, to provide a straightforward method to evaluate the burnout resistance of concrete members.
- Finally, future work should explore the question of the target performance objective. What is the objective when designing a concrete structure for fire? As understanding of the structural response under natural fires improve, guidance should be provided, based on rational considerations, on the objectives of the design as a function of the characteristics of the building. While the derivation of simple methods and tabulated data to easily evaluate the burnout resistance is a necessary step, it is also important to establish the level of burnout resistance that should be required for different structural members. Such an effort should probably rely on probabilistic risk assessment and the consideration of cost and benefit of investing in enhanced structural fire safety to maintain stability throughout a fire event.

References

[1] ASTM International, ASTM E119-16a Standard Test Methods for Fire Tests of Building Construction and Materials, ASTM International, West Conshohocken, PA, 2016.

[2] CEN (European Committee for Standardization), EN 1992-1-2 Eurocode 2: Design of Concrete Structures - Part 1-2: General Rules – Structural Fire Design, Brussels, Belgium, 2005.

[3] J.F. Cadorin, D. Pintea, J.C. Dotreppe, J.M. Franssen, A tool to design steel elements submitted to compartment fires - OZone V2. Part 2: Methodology and application, Fire Safety Journal. 38 (2003) 429–451. https://doi.org/10.1016/S0379-7112(03)00015-8.

[4] A.I. Bartlett, R. McNamee, F. Robert, L.A. Bisby, Comparative energy analysis from fire resistance tests on combustible versus noncombustible slabs, Fire and Materials. 44 (2020) 301–310. https://doi.org/10.1002/fam.2760.

[5] CEN (European Committee for Standardization), EN 1991-1-2 Eurocode 1: Actions on structures - Part 1-2: General actions - Actions on structures exposed to fire, CEN, Brussels, Belgium, 2002.

[6] J.-M. Franssen, T. Gernay, Modeling structures in fire with SAFIR®: theoretical background and capabilities, Journal of Structural Fire Engineering. 8 (2017) 300–323. https://doi.org/10.1108/JSFE-07-2016-0010.

[7] T. Gernay, J.-M. Franssen, A performance indicator for structures under natural fire, Engineering Structures. 100 (2015) 94–103. https://doi.org/10.1016/j.engstruct.2015.06.005.

[8] T. Gernay, Fire resistance and burnout resistance of reinforced concrete columns, Fire Safety Journal. 104 (2019) 67–78. https://doi.org/10.1016/j.firesaf.2019.01.007.

[9] M. Law, A Review Of Formulae For T- Equivalent, Fire Safety Science. 5 (1997) 985–996. https://doi.org/10.3801/iafss.fss.5-985.

[10] A. Sauca, Development and implementation of a methodology for hybrid fire testing applied to concrete structures with elastic boundary conditions, University of Liege, Belgium, 2017.

[11] D.T. Pham, N. Pinoteau, M. Yang, P. de Buhan, P. Pimienta, R. Mège, Full-scale fire test on a high-rise RC wall, Engineering Structures. 227 (2021) 111435. https://doi.org/10.1016/J.ENGSTRUCT.2020.111435.

[12] L. Lim, A. Buchanan, P. Moss, J.M. Franssen, Numerical modelling of two-way reinforced concrete slabs in fire, Engineering Structures. 26 (2004) 1081–1091. https://doi.org/10.1016/J.ENGSTRUCT.2004.03.009.

[13] T. Gernay, A. Millard, J.M. Franssen, A multiaxial constitutive model for concrete in the fire situation: Theoretical formulation, International Journal of Solids and Structures. 50 (2013) 3659–3673.

[14] T. Gernay, J.M. Franssen, A formulation of the Eurocode 2 concrete model at elevated temperature that includes an explicit term for transient creep, Fire Safety Journal. 51 (2012) 1–9. https://doi.org/10.1016/J.FIRESAF.2012.02.001.

[15] C. Maluk, G. Pietro Terrasi, L. Bisby, A. Stutz, E. Hugi, Fire resistance tests on thin CFRP prestressed concrete slabs, (n.d.). https://doi.org/10.1016/j.conbuildmat.2015.10.031.

[16] F. Dumont, E. Wellens, T. Gernay, J.-M. Franssen, Loadbearing capacity criteria in fire resistance testing, Materials and Structures. (2016). https://doi.org/10.1617/s11527-016-0807-7.

[17] ACI 216, Code Requirements for Determining Fire Resistance of Concrete and Masonry Construction Assemblies, Farmington Hills, MI, 2017. www.concrete.org.